AD-757 088

Tunable 10 Micron Laser, an Integrated Optics Approach to Infrared Gas Lasers

Rockwell International Corp.

prepared for

Office of Naval Research
Advanced Research Projects Agency

FEBRUARY 1973

Distributed By:

NTIS
National Technical Information Service
U. S. DEPARTMENT OF COMMERCE

AD 757088

C72-650.10/501

INTERIM TECHNICAL REPORT

TUNABLE 10 MICRON LASER

AN INTEGRATED OPTICS APPROACH TO INFRARED GAS LASERS

BY

D. B. Anderson
R. Shubert

DISTRIBUTION STATEMENT A
Approved for public release;
Distribution Unlimited

February 26, 1973

Prepared for the Office of Naval Research
Contract N00014-72-C-0505

1 June 1972 to 31 December 1972 - $49,550
Sponsored By
Advanced Research Projects Agency
ARPA Order #1806, dated 2-9-72

Reproduced by
NATIONAL TECHNICAL
INFORMATION SERVICE
U S Department of Commerce
Springfield VA 22151

D D C
RECEIVED
MAR 19 1973

Electronics Research Division
Rockwell International
3370 Miraloma; Anaheim, California 92803

UNCLASSIFIED
Security Classification

DOCUMENT CONTROL DATA - R & D

(Security classification of title, body of abstract and indexing annotation must be entered when the overall report is classified)

1. ORIGINATING ACTIVITY (Corporate author)
ROCKWELL INTERNATIONAL CORPORATION

2a. REPORT SECURITY CLASSIFICATION
Unclassified

2b. GROUP

3. REPORT TITLE
TUNABLE 10 MICRON LASER, AN INTEGRATED OPTICS APPROACH TO INFRARED GAS LASERS

4. DESCRIPTIVE NOTES (Type of report and inclusive dates)
Interim Technical Report, June 1, 1972 - February 28, 1973

5. AUTHOR(S) (First name, middle initial, last name)
D. B. Anderson
R. Shubert

6. REPORT DATE
February 26, 1973

7a. TOTAL NO. OF PAGES
70

7b. NO. OF REFS
45

8a. CONTRACT OR GRANT NO.
Contract N00014-72-C-0505

b. PROJECT NO.
ARPA Order No. 1806 dtd 2-9-72

c.

d.

9a. ORIGINATOR'S REPORT NUMBER(S)
C72-650.10/501

9b. OTHER REPORT NO(S) (Any other numbers that may be assigned this report)

10. DISTRIBUTION STATEMENT
Distribution of this document is unlimited.

11. SUPPLEMENTARY NOTES
Prepared for Office of Naval Research

12. SPONSORING MILITARY ACTIVITY
Sponsored by Advanced Research Projects Agency

13. ABSTRACT
Current progress toward the development of a tunable CO_2 laser employing an integrated optics approach is delineated herein. Design parameters for application as a local oscillator in optical heterodyne receiver are emphasized with tunability to accommodate the large doppler offset. The integrated optics approach employs a non-uniform distributed iterative passive waveguide in close proximity to a planar active gas waveguide to form the resonant circuit. Backward wave Bragg diffraction coupling is employed between the active gas waveguide and the passive feedback waveguide. Transverse gas flow and transverse excitation are considered. The characteristics of non-uniform distributed feedback laser ring resonant circuits are analyzed employing a coupled mode approach. One important virtue of the distributed hetero-feedback structure analyzed is the provision for design-control of the laser longitudinal mode spectrum to accommodate requirements for a wide tuning range. Production of the required backward wave Bragg diffraction couplers and the passive feedback waveguide by photolithographic techniques and demonstration of their operation has been successful. A 0.6 mm diameter bore capillary waveguide laser has been demonstrated. The production of a continuous uniform plasma discharge at the required high pressures to accommodate tuning in the thin planar active gas waveguide is the most serious problem encountered. Both DC and RF-excitation had been employed yielding concentrated arcs in the thin waveguide section. Various means to produce a continuous uniform plasma discharge in the thin waveguide cross section are continuing to receive attention.

DD FORM 1 NOV 65 1473 (PAGE 1) PLATE NO. 21856

S/N 0102-014-6600

UNCLASSIFIED
Security Classification

Unclassified
Security Classification

14 KEY WORDS	LINK A ROLE	LINK A WT	LINK B ROLE	LINK B WT	LINK C ROLE	LINK C WT
CO_2 gas laser						
Integrated optics						
Distributed feedback						
Backward wave Bragg diffraction coupler						
Capillary waveguide laser						
Planar plasma discharge						
Longitudinal resonant modes						

DD FORM 1 NOV 65 1473 (BACK)
(PAGE 2)

i-a

Unclassified
Security Classification

C72-650.10/501

INTERIM TECHNICAL REPORT

TUNABLE 10 MICRON LASER
AN INTEGRATED OPTICS APPROACH TO INFRARED GAS LASERS

by

D. B. Anderson
R. Shubert
(714) 632-1889

February 26, 1973

DISTRIBUTION STATEMENT A
Approved for public release;
Distribution Unlimited

Prepared for the Office of Naval Research
Contract N00014-72-C-0505

1 June 1972 to 31 December 1972 - $49,550
Sponsored By
Advanced Research Projects Agency
ARPA Order #1806, dated 2-9-72

The views and conclusions contained in this document are those of the authors and should not be interpreted as necessarily representing the official policies, either expressed or implied, of the Advanced Research Projects Agency or the U. S. Government.

Reproduction in whole or in part is permitted for any purpose of the United State Government.

Distribution of this document is unlimited

Electronics Research Division
Rockwell International
3370 Miraloma; Anaheim, California 92803

D D C
RECEIVED
MAR 19 1973

SUMMARY

The development of a tunable CO_2 laser employing an integrated optics approach to its construction is delineated herein. Current progress toward the demonstration of operation, technical problems encountered, and the approach proposed to incorporate the tunable feature are included. The apposite laser design parameters for application as a local oscillator for a tunable optical heterodyne receiver are emphasized. Tunability is required to accommodate the large doppler shifts encountered with high velocity targets or in active sensor systems on high velocity vehicles.

The integrated optics approach employs a nonuniform distributed iterative passive waveguide in close proximity to a planar active gas waveguide to form the resonant circuit. Backward wave Bragg diffraction coupling is employed between the active gas waveguide and the passive feedback waveguide. Transverse gas flow and transverse excitation are considered as opposed to the longitudinal configuration of a capillary waveguide laser. Collinear Bragg diffraction by surface elastic (Rayleigh) waves in the passive feedback waveguide is proposed to achieve the wide tuning range.

The characteristics of nonuniform distributed feedback laser ring resonant circuits are analyzed employing a coupled mode approach. One important virtue of the distributed hetero-feedback laser structure analyzed is the provision for design-control of the laser longitudinal mode spectrum to accommodate requirements for a wide tuning range. Production of the required backward wave Bragg diffraction couplers and the passive feedback waveguide by photolithographic techniques and demonstration of their operation has been successful.

Because the active gas waveguide is thin (100 microns) it was deemed necessary to experimentally verify increased gain due to the close proximity of the waveguide walls. This was done by extending the capillary waveguide laser art, using a 0.6 mm diameter bore.

The production of a continuous uniform plasma discharge at the required high pressures to accommodate tuning in the thin planar active gas waveguide is the most serious problem encountered. Both DC and RF-excitation had been employed yielding concentrated arcs in the thin waveguide section. Various means to produce a continuous uniform plasma discharge in the thin waveguide cross section are continuing to receive attention. The thin plasma discharge chamber investigated differs drastically from that of the large chambers employed for transverse excited atmospheric CO_2 laser designs which employ fast-flow and only operate in a pulsed mode.

Recommendations altering the design to alleviate problems encountered with the concentrated arcs are proposed in exchange for problems due to the increase of the active waveguide thickness and its coupling to the passive feedback waveguide via the contra-directional couplers.

TABLE OF CONTENTS

	PAGE
SUMMARY	iii
I. INTRODUCTION	1
A. PROGRAM OBJECTIVE	1
B. CAPILLARY WAVEGUIDE LASER ART	3
C. DISTRIBUTED FEEDBACK LASERS (DFB)	5
II. TECHNICAL DISCUSSION	9
A. AN INTEGRATED OPTICS APPROACH FOR A TUNABLE CO_2 LASER	9
B. PRINCIPLES OF DISTRIBUTED FEEDBACK COUPLING IN WAVEGUIDES	17
1. The Concept of Mode Coupling on Periodic Structures	17
2. Waveguide Eigenfunctions	20
3. Coupled Mode Solutions for the Bifurcated Cavity	23
4. Complex Reflection Coefficients of DFB Structures	29
C. DISTRIBUTED FEEDBACK CO_2 LASERS	35
1. The Concept of Laser Miniaturization	35
2. Resonance Modes in Periodic Active Media	36
3. Laser Spectra Approximations	41
D. EXPERIMENTAL EFFORT	49
1. Capillary Waveguide CO_2 Laser	49
2. CO_2 Planar Plasma Discharge	51
3. Backward Wave Bragg Diffraction Coupler	55
III. REVIEW	63
A. CONCLUSIONS AND RECOMMENDATIONS	63
B. REFERENCES	65

I. INTRODUCTION

A. PROGRAM OBJECTIVE

Our defense establishment continues to require from technology an ever-increasing sensitivity and resolution improvement from active sensor systems. The emission from a CO_2 laser is regarded by system engineers as an excellent source for active sensors because (1) it is capable of enormous power outputs realized efficiently, (2) its wavelength is in a superior atmospheric "window" which is least affected meteorologically, and (3) the associated tolerances required are commensurate with high gain apertures.

The superheterodyne receiver provides the ultimate sensitivity in the IR spectral region. Wideband performance is required for high-range resolution while frequency stability is required for high-spatial resolution derived from transverse Doppler signal processing. Many targets of interest to our defense move at high velocity and, thus, introduce a Doppler shift in the received signal. The received baseband signal with Doppler extends into the microwave region. The photodetector response is severely limited in the microwave region; therefore, for a superheterodyne system, a local oscillator is required which can be tuned sufficiently to accommodate the Doppler offset such that the available detector response bandwidth can be fully utilized to achieve resolution without degradation from noise due to excess bandwidth.

Typical laboratory CO_2 lasers produce tens of watts power output whereas a heterodyne receiver local oscillator only requires a few tenths of watts. These typical laboratory CO_2 lasers employ comparatively long Fabry-Perot resonators to achieve the higher power output. However, the close proximity of the longitudinal Fabry-Perot modes severely limits the tuning range. Current engineering practice to increase the tuning range by reducing the Fabry-Perot length generally lowers the power output to a level insufficient for a tracking (monopulse) heterodyne receiving system. Further, these laboratory CO_2 lasers operate at a pressure of a

few tens of Torr which produces a collision-broadened linewidth comparable to the longitudinal Fabry-Perot mode period, thus producing a single emission line. A substantial increase of pressure approaching 1/2 an atmosphere is essential to collision-broaden the emission linewidth sufficiently to accommodate a tuning range commensurate with the Doppler offset. However, the Fabry-Perot length must be severely limited to achieve a wide tuning range and single mode output. High pressure operation also leads to an increased power generation per unit volume. The scaling properties of tube-confined gas discharge plasmas[1] suggest the possibility of operating at high pressures.

An effort to develop a tunable 10 micron laser for application as a local oscillator and to provide a sufficiently wide unambiguous tuning range to accommodate a large Doppler offset is delineated in this report. The approach being developed has its roots in the capillary waveguide laser art. However, it is unique because it employs a planar configuration compatible with the processing techniques for integrated circuits. The integrated optics approach to far infrared gas lasers and the supporting theoretical effort together with experiments to demonstrate the concept using CO_2 is documented herein. The basic approach to achieve wide unambiguous tuning is included. However, the experimental development is relegated to a later phase.

The integrated optics approach employs a distributed iterative waveguide in close proximity to the active gas to form the resonant circuit. Bragg backward wave diffraction coupling is employed between the active gas waveguide and the passive feedback waveguide. Transverse gas flow and transverse discharge excitation are considered as opposed to the longitudinal configuration of a capillary waveguide laser. Collinear Bragg diffraction by surface elastic (Rayleigh) waves in the passive feedback waveguide is proposed to achieve the wide tuning range.

B. CAPILLARY WAVEGUIDE LASER ART [6-7]

Use of the hollow dielectric waveguide (capillary) in lasers was first suggested by Marcatili and Schmeltzer[2] as a confinement structure for the gas discharge and the emitted light. It was first demonstrated by Smith[3] using He/Ne in the far red. In the 1 μ region, a hollow glass capillary tube with bore diameter of 2 mm exhibits a propagation loss of 2 dB/Km for the EH_{11} mode. Similarly, for an aluminum tube at the same wavelength with a 0.5 mm diameter, the transmission loss is also 2 dB/Km for the TE_{01} mode. Although these low losses are attractive, stringent requirements are imposed upon the bend radius of these guides. If the propagation loss is allowed to increase by a factor of two by the bend, the minimum radius for the hollow glass capillary is 10 Km! Therefore, use of a capillary waveguide, together with Fabry-Perot reflectors for field confinement in a laser resonator, imposes stringent mechanical alinement requirements.

Interest in the capillary waveguide configuration arises from the desirable effect of the waveguide walls upon the active gas, with the result that (1) a significant increase in gain is realized,[4] (2) an increased emission linewidth, (3) an increased volumetric power generated and (4) an increased saturation parameter.[5] These desirable characteristics evolve from a favorable de-excitation of the CO_2 by the walls, operation at an increased optimum pressure and reduced plasma temperature because of improved thermal conductivity to the walls. A comparison of published CO_2 laser parameters including gain, power density and saturation parameter is summarized in Table I. Results for a capillary configuration at two temperatures, a high flow rate configuration, and the conventional approach are indicated with the corresponding plasma tube bore diameter and the plasma tube material. The effect of using the capillary waveguide approach upon the capillary gas dynamics and thus the gain is startling. The power density and saturation parameters are dramatically increased by the capillary configuration because of the pressure scaling inversely with the diameter. The effect of temperature and the substitution of a high thermal conductive capillary (BeO) is dramatic. In the

capillary waveguide tubes, the optimum current density is approximately 100 times larger than in conventional tubes, resulting in a larger power input per unit length (300 W/m) and in available volumetric power output. In general, the small diameter plasma tube has led to an increased optimum pressure with a corresponding increase of the emission linewidth and required electric field to excite the plasma. The gradient of pressure throughout the capillary is such as to inhomogeneously collision-broaden the emission line through the capillary length.

TABLE 1

CO_2 LASER PARAMETERS

Type	Gain dB/M	Power Density W/cm^3	Saturation Parameter W/cm^2	Tube Dia. mm
Capillary				
* SiO_2 230°K	21			0.6
[6] BeO 230°K	28	30	6300	1
300°K	19	18	3400	1
[7] SiO_2 230°K	37	15	3600	1
300°K	24	9	2100	1
* SiO_2 240°K	32	3		1
300°K	19			1
[8] SiO_2 300°K	12		4400	2
[9] SiO_2 300°K		9	~ 100	3.3
High Flow	4	9	500	13
Conventional	11	.25	100	13
	20	1.4		5

* Data derived as a part of this program.

As a part of this effort, several SiO_2 capillary lasers were constructed, characterized and their operation demonstrated. The smallest plasma tube of 0.6mm dia. yielded a measured gain of 21dB/M at 230°K. Another plasma tube of 1.0mm dia. yielded a measured gain of 32dB/M at 240°K and 19db/M at 300°K. For the 0.6mm dia., the capillary wall was

1.0mm. The effect of the large pressure drop (100 Torr) in the 0.6mm capillary is, presumably, the cause for this reduced measured gain. Further, no clear optimum pressure was observed. For the 1.0mm bore, the capillary wall thickness was 4mm. These gain measurements are approximately 5dB less than comparable results of Bridges[7] presumably due to increased gas temperature due to the larger capillary wall thickness and due to the use of standard capillary instead of precision bore capillary tubing.

Our experience derived from using the circular capillary configuration has emphasized the critical requirement for cooling the CO_2:N_2:He mixture. The confined plasma discharge requires an effective thermal sink as demonstrated by Burkhardt, et al,[6] using BeO ceramic. Further, the problems associated with the high-voltage gradients, the high-pressure gradients and the high-temperature gradients which arise as a result of the confinement in the capillary configuration all emphasize the desirability to develop an alternate approach. Further, the requirement for a wide tuning range emphasizes that the collision-broadened linewidth must be uniform throughout the gain region. Therefore, a waveguide approach is followed which provides for a transverse flow of gases and a transverse excitation of the plasma.

C. DISTRIBUTED FEEDBACK LASERS (DFB)[10-19]

Concurrent with the development of capillary waveguide lasers has been the development of distributed waveguide periodic structures incorporated in the active lasing material as a feedback mechanism. Conventional lasers employ a Fabry-Perot reflector system with a portion of the resonant volume containing the active lasing medium as the feedback mechanism. The distributed feedback concept depends upon the constructive, cumulative reflection from a periodic structure or grating which extends throughout an active planar laser medium or immediately adjacent to the active medium. A distributed feedback is an attractive means to realize a resonant structure in the plane of an integrated optical circuit. The distributed feedback provides important advantages which include high spectral purity, design controllable, longitudinal mode and several means to effect tuning of the laser emission output.

Thus far, the demonstration of distributed feedback lasers has been confined to high-gain laser media (dye)[10-13] The validity of the DFB concept has been adequately demonstrated and its emission spectrum characterized under pulse conditions. However, it has as yet not been demonstrated with an active material in a continuous operating mode. Most experimenters have employed a blazed diffraction grating or a grating produced in a photographic emulsion adjacent to the active laser material. They have also employed the interference of two pump beams to produce a grating of excitation in the active laser material. Two methods of tuning of these structures have been demonstrated. The first by changing the angular orientation of the interfering pump beams has changed the active grating period and, thus, the emission wavelength.[11] The other approach has employed an anisotropic substrate confining the active laser medium such that the evanescent field penetrating the substrate is affected by the orientation.[18]

The theory for distributed feedback dielectric waveguides, backward wave scattering from periodic structures and the spectral characteristics is an important analytical conception which has evolved from this effort. The analyses are an extension of the current literature to include structures wherein the active and passive feedback waveguide and the backward wave diffraction couplers are separate design-controllable functions. Results of this analysis are employed in a later section to describe apposite characteristics of our approach to a tunable integrated CO_2 laser.

After a heuristic description of our integrated optics approach to a tunable CO_2 laser in Section II, an analysis of the distributed feedback structure contained therein is presented. The backward wave Bragg diffraction coupling of guided modes in a bifurcated waveguide structure with periodic perturbation on the waveguide dimensions and the spectral characteristics of this planar resonant structure are presented. Marcuse[13] presents an analytical treatment of backward Bragg scattering in hollow dielectric waveguide lasers using a planar geometry. However, he has considered only symmetrical waveguide structures. The type of geometry discussed in this report, however, requires the knowledge of the characteristics of backward wave coupling on asymmetrical structures of

the type considered by Shubert.[20] Kogelnik[19] has performed a coupled mode analysis of DFB lasers and derived both threshold gain parameters and lasing frequencies for the case when the feedback grating is continuous over the entire length of the active region. The distributed hetero-feedback (DHFB) structure wherein the feedback is a discontinuous function along the laser structure is considered as a design-controllable means to alter the gain and spectral characteristics. The specific case considered of non-uniform feedback is that of a central gap in the grating.

Section II-B considers the basic principles of DFB coupling between modes of the bifurcated guide region composed of both the active gas cavity and the feedback waveguide. Coupling constants between oppositely travelling modes are derived as a function of waveguide parameters. Spectral characteristics of the periodic perturbations are examined in detail and complex reflection coefficients derived. Section II-C presents the coupled mode analysis for a general DFB structure where a control gap is included into a continuous-feedback grating. Approximate eigenvalue equations are presented which illustrate the variation of the laser frequency spectrum with the grating parameters for the low gain CO_2 case.

II. TECHNICAL DISCUSSION

A. AN INTEGRATED OPTICS APPROACH FOR A TUNABLE CO_2 LASER

The design approach currently being implemented and investigated differs radically from that of current practice relating to the CO_2 capillary laser. The design has emphasized a planar active waveguide structure arranged to provide transverse flow and excitation of the CO_2:N_2:He gas mixture instead of the collinear confinement by the capillary. Another design feature incorporates an active waveguide containing the CO_2 plasma discharge, paralleled with a passive feedback waveguide wherein both waveguides are coupled via backward wave Bragg diffraction couplers to form a ring resonant circuit (no area). Characterization of our active/passive waveguide ring with contradirectional couplers is delineated in detail in a following section.

The transverse and longitudinal cross-sections of the tunable integrated CO_2 laser as conceived are illustrated in Figures 1 and 2. The full structure in its entirety is delineated. However, at this point in the program only certain facets have been developed and others are contingent upon further investigation. These include techniques to achieve a uniform plasma discharge and later the incorporation of techniques to tune the laser. It employs entirely a planar processing technology. Referring to the transverse cross-section, the active waveguide contributing to the gain is a rectangular section 100 μ in height and 3000 μ in width. The length of the active waveguide indicated in Figure 2 is 9 cm.

The thin film feedback waveguide to be formed by evaporation of a II-VI semiconductor such as ZnSe will be approximately 3 μ thick and 3000 μ wide. Two techniques are employed to create the backward wave Bragg diffraction couplers. They include either direct ion milling on the surface or ion milling of a gold superstrate film on the ZnSe film to produce transverse conductive bars as a grating. The grating and control of its period are formed by a holographic technique,[15] i.e., the interference of two krypton laser beams.

The transverse cross-section is composed of two parallel, adjacent planar substrates. The upper section contains the CO_2:N_2:He gas ports connected to two parallel chemically-etched channels serving as a gas distribution manifold on each side of the active waveguide. The direction of gas flow is illustrated in Figure 2. The upper superstrate forms the gas

Preceding page blank

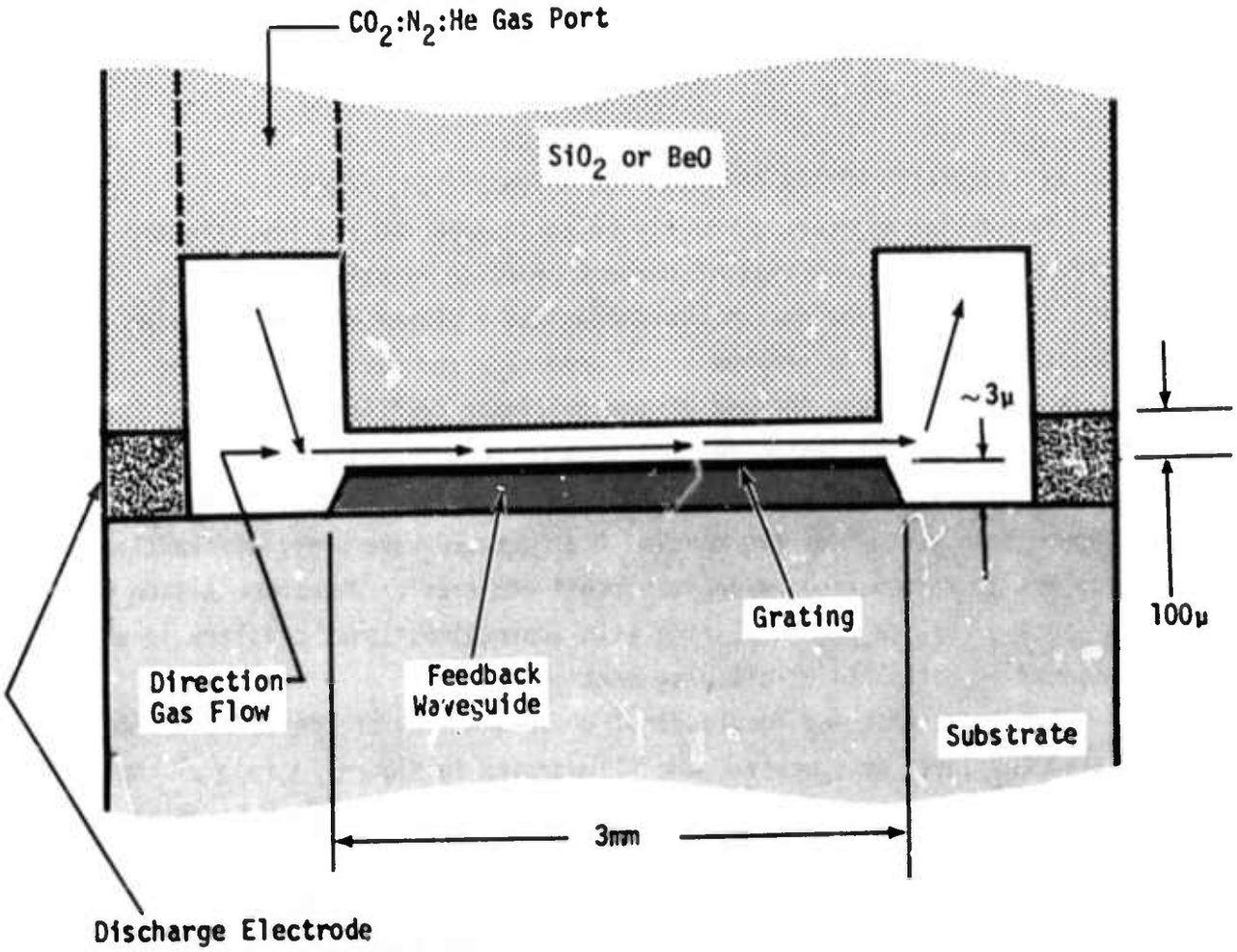

Figure 1. Transverse cross-section of the integrated optics approach to a tunable CO_2 laser indicating the active hollow and dielectric feedback waveguide.

manifold and one wall of the active hollow waveguide. It has been fabricated from either fused silica or, more preferably, from polycrystalline BeO. A ring is incorporated for bonding of the super and substrates.

It is the intent that either DC or RF-excitation be employed. If DC-excitation is employed, the inner walls of the gas manifold are metalized to produce high surface resistivity and a uniform field between cathode and anode. For RF-excitation, the bonding ring is intended as the RF coupling loop. Thus far, the excitation method and electrode design approach are not defined, be-

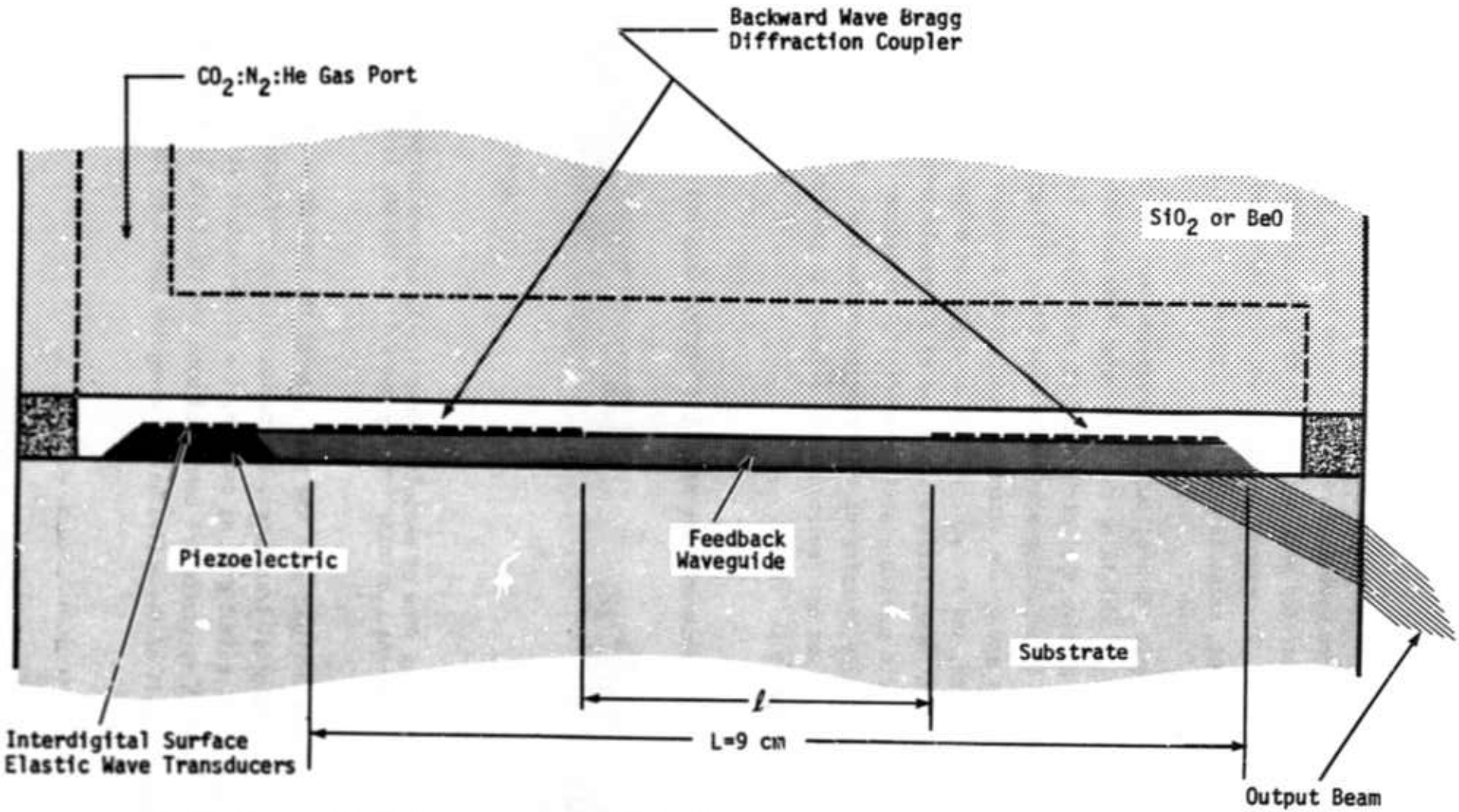

Figure 2. Longitudinal cross-section of the integrated optics approach to a tunable CO_2 laser indicating the active hollow waveguide, dielectric feedback waveguide, and backward wave Bragg diffraction couplers.

cause attempts to achieve a continuous-uniform discharge throughout the active hollow waveguide region have not been successful. In general, concentrated arcs are usually observed at the necessary high pressure. At reduced pressure, and with increased hollow waveguide height, reasonably uniform discharges are obtained.

Referring to the longitudinal cross-section, the hollow active waveguide containing the transverse flow and discharge is bounded by a passive dielectric feedback waveguide. Each end of the assembly incorporates a backward wave Bragg diffraction coupler. One end of the assembly incorporates a change of grating period, and as such, is used as a grating output coupler. The other end incorporates a small pad of a piezoelectric either ZnO or AlN. A gold surface elastic interdigital transducer is photolithographically transferred to piezoelectric surface. This transudcer as yet not implemented is intended to provide the means to tuning the laser.

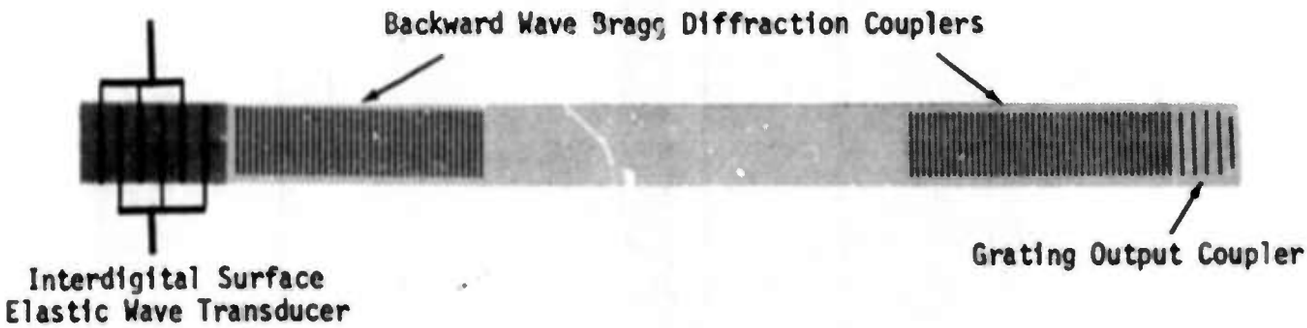

Figure 3. Plan View of photolithographically defined patterns on the substrate forming one wall of the CO_2 laser.

Figure 3 illustrates the plan view of the surface elastic wave interdigital transducer, the backward Bragg diffraction coupler, the output grating coupler, the piezoelectric island and feedback waveguide are deposited upon the substrate to form the opposite wall of the active hollow waveguide confining the plasma discharge.

The planar structure serving as a substrate for the piezoelectric interdigital transducer, the feedback waveguide, and the contradirectional coupler must employ a material transparent at 10 microns if the output is taken via a grating through the substrate. Several choices are available. They include single crystal NaF, polycrystalline ZnS, NaCl, and CdTe. The feedback waveguide deposition is a polycrystalline film. The piezoelectric film incorporates orientation in a single plane via the deposition technique. NaCl is an unsatisfactory substrate from the point of view of propagating a surface elastic wave in the dielectric feedback waveguide because of its extremely high acoustic attenuation. Realization of the backward wave Bragg diffraction couplers is preferred in an undulated surface configuration, but may infact be more easily produced as a gold bar grating. Comparative measurements of the loss and scattering of the diffraction efficiency will determine the appropriate approach.

The design of the active CO_2 waveguide cross-section is currently set as 100 x 3000 μ with a length of 10 cm. The optical field containment within the active waveguide is achieved in height by the walls and in width by the grating. Field containment in the passive feedback waveguide is achieved by the dielectric interface. The feedback waveguide thickness and its refractive index has important effect upon the longitudinal mode spectra. Using a conservative estimate of the volumetric power density of 10 W/cm^3 (see Table 1), the expected laser power output should be approximately 300 mW. If additional power is required, the waveguide width can be increased. The waveguide length could also be increased to achieve additonal gain and power output; however, at the expense of limiting the longitudinal mode spectrum period and the maximum tuning range.

Use of transverse flow through the restricted channel 3 mm long with a cross-section of 100 μ x 10 cm should provide a more homogeneous excitation method in comparison to the capillary

approach. The collision-broadened linewidth should be uniform throughout the active waveguide region. The excitation field should be uniform throughout the active waveguide region. The excitation field should be substantially reduced. Operation at approximately 300 Torr will be required to obtain the necessary collision-broadened linewidth. One serioud problem is being encountered; i.e., obtaining a uniform discharge throughout the active waveguide.

A crucial feature in the design for wide range tuning is the appropriate control of the longitudinal mode spectrum, in order that a single unambiguous emission line is generated for use in optical heterodyning. The longitudinal mode spectrum of this integrated CO_2 laser design containing an active waveguide coupled with a passive feedback waveguide differs from that of conventional Fabry-Perot resonators. The longitudinal mode period is C/2L. To provide for tuning out to 1.5 GHz requires the length to be reduced such that marginal power output may be available. For a continuous distributed feedback waveguide extending throughout the active region wherein propagation in both directions is contained within the same waveguide.[13] The continuous grating throughout the length, or limited to regions at the extremities, provides continuous circulation. The grating period becomes a dominant frequency determining parameter. The grating, however, also couples the various propagating transverse mode orders together.[24] When a separate dielectric feedback waveguide is provided, and a discontinuous grating is employed, as in this program, the longitudinal mode period may be increased beyond C/2L. In this case, the spectral width is critically dependent upon the active gain and the magnitude of the perturbing feedback circuit. The backward wave Bragg diffraction coupler location in the ring perimeter is offset. This is due to the use of a dielectric feedback waveguide over the longer portion of the ring. The asymmetry[25] thus introduced and the dispersion of the waveguide and the frequency selectivity of the contradirectional couplers all enter into control of the longitudinal mode spectrum. Specific details delineating this frequency selectivity, the contradirectional coupler design efficiency are summarized in Sections IIB and IIC.

The interaction of a travelling or standing surface elastic wave within and collinear with an optical waveguide produces similar phenomena to that in a distributed feedback waveguide or a forward/backward wave Bragg diffraction coupler. Surface elastic waves are of interest because the field containment, like that of dielectric optical waveguide, can produce strong, efficient interactions. Further, changing of the surface elastic wavelength will alter the waveguide dispersion and radiation fields. Bragg diffraction has been produced dielectric waveguide by surface elastic waves[21] and has been used in a collinear form for mode conversion.[22] It has been proposed[20,23] in a collinear configuration to produce a radiation beam which may be scanned by altering the surface elastic wave frequency.

Tuning of the integrated laser can be achieved by employing a travelling or standing surface elastic wave propagating through the feedback waveguide. The dispersion of planar dielectric waveguide used in the feedback circuit containing the surface elastic wave as a periodic perturbation is illustrated in Figure 4. It shows a Brillouin diagram for planar dielectric waveguide. The modes not identified are $TE_0TM_0TE_1TM_1TE$ . . . . . The dispersion of the planar dielectric waveguide is confined between free-space (c) and the phase velocity within the bulk dielectric (refractive index). The effect of the periodic perturbation as the Bragg frequency is noted as a stop band. This is the condition for the backward wave or contradirectional coupler. At this frequency, the waveguide is cutoff, reflecting the radiation.[26] At frequencies removed from the stop band, the waveguide is transparent and may be used to phase-match nonlinear interactions.[27-28] The region wherein the travelling surface elastic wave perturbs the dielectric waveguide dispersion is indicated in Figure 4. Changes of the surface elastic wavelength and its amplitude will control the dispersion of the feedback waveguide and in turn the integrated CO_2 laser emission wavelenth. The frequency shift is the integrated effect of all phase

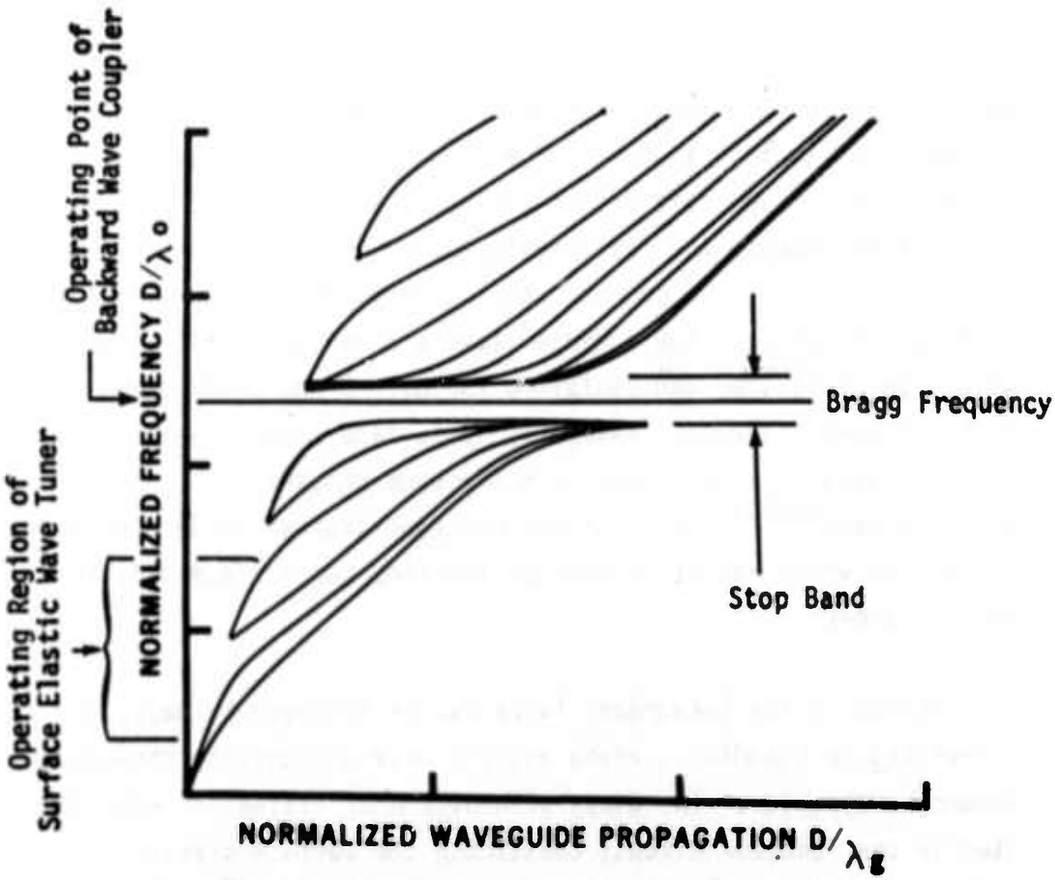

Figure 4. Dispersion of planar dielectric waveguide containing a periodic perturbation.

shifts introduced throught the entire feedback waveguide. Rapid tuning of the integrated CO_2 laser is limited by the time required for the elastic wave to propagate through the delay line and be replaced by a second different frequency.

Features for the above CO_2 laser design include the full use of planar processing fabrication techniques and use of transverse excitation and gas flow relative to the optical path. Particular attention has been given to continuous operation at relatively high pressure for its eventual use as a tunable local oscillator for optical heterodyne. A detailed analysis of the distributed feedback waveguide, the backward wave Bragg diffraction coupler and their spectral characteristics follows in the next section:

B. PRINCIPLES OF DISTRIBUTED FEEDBACK COUPLING IN WAVEGUIDES

1. The Concept of Mode Coupling on Periodic Structures

Marcuse[29] has extensively investigated the scattering of optical guided waves from slab-type waveguides using an orthogonal modal expansion of the characteristic modes of the unperturbed waveguide. His technique was applied primarily to determine the scattering losses from random perturbations on the waveguide walls of a symmetrical slab structure. This technique serves as the basis for the theoretical discussion here and is considered briefly to establish the notation.

We consider the CO_2 laser cavity exemplified in Figure 5 containing both the plasma region and a thin-film feedback waveguide through which energy passes during part of the round-trip cycle. The structure under consideration here differs from DFB laser geometries considered by Kogelnik[19] in that we include a bifurcated cavity and a semi-continuous distributed feedback grating both to be used for tuning and control of the laser output. The semi-continuous grating is that shown in Figure 5 where the central portion of length ℓ has been removed from a total grating length L.

Basic operation of the structure is similar to that of the DFB coupling process discussed by Kogelnik, Bjorkholm and Shank[16,18,19] and Zory [17] except that backward Bragg diffraction couples a wave travelling towards the grating from the gas cavity to a wave travelling away from the grating in the thin-film waveguide and vice-versa. The cavity shown in the figure may support trapped waves of low loss if grazing incidence rays are involved. In addition, guided modes may exist on the thin film structure consisting, for example, of GaAs on NaF.

The following analysis illustrates the basic characteristics of coupling between guided modes travelling in opposite directions when the waveguide region is perturbed periodically. If only TE waves are

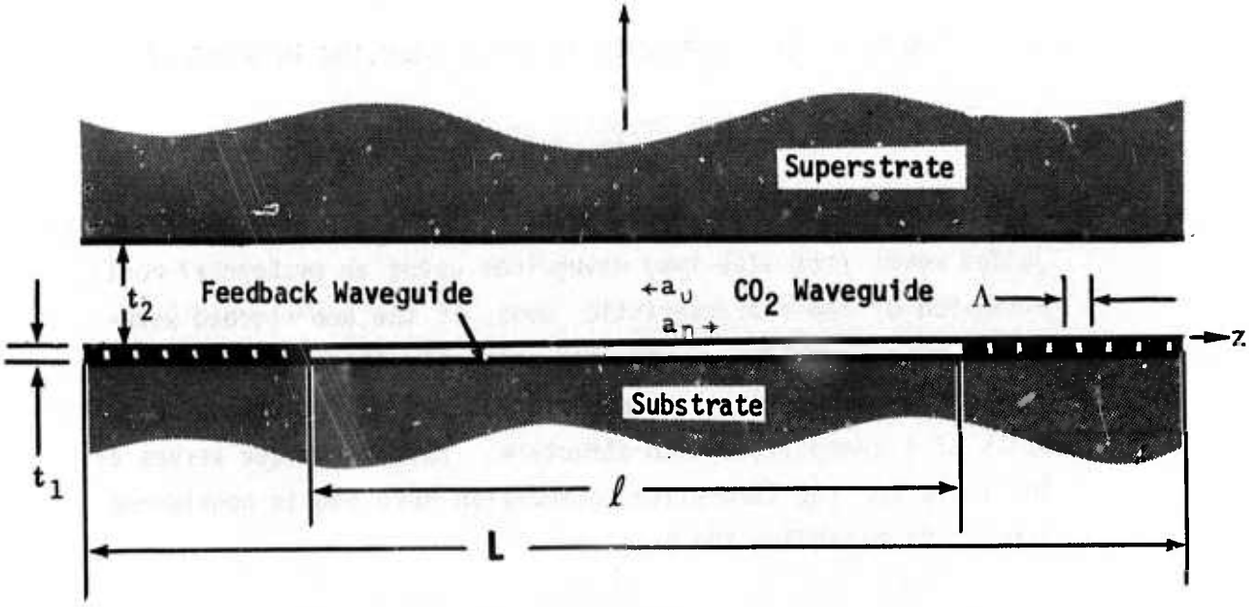

Figure 5. Geometry of the distributed feedback resonator with bifurcated guide and semi-continuous feedback grating

considered for which the electric field vector will be parallel to the perturbations in the waveguide, then the wave equation for fields propagating in the active guide becomes

$$\left[\nabla^2_{xz} + k^2(n + \Delta n(x,z))^2\right] E_t(x,z) = 0 \qquad (1)$$

where $\Delta n(x,z)$ represents the functional form of the perturbation on the waveguide in either its local thickness or refractive index and E_t is the total electric field.

The total y-directed electric field may be represented by a summation over all discrete modes E_n of the thin-film waveguide and the discrete modes E_ν of the cavity according to

$$E_t(x,z) = \sum_{n,\nu} a_{n,\nu}(z)\, E_{n,\nu}(x,z) \qquad (2)$$

where the subscripts n and ν are here written together in condensed form. The individual modes propagate along the z-direction according

to $\exp(i\beta z-\omega t)$ and have magnetic field components expressed by

$$H_x = \frac{i}{\omega\mu}\frac{\partial E_t}{\partial z} \tag{3}$$

$$H_z = \frac{i}{\omega\mu}\frac{\partial E_t}{\partial x} \quad . \tag{4}$$

The coupled mode equations involving the amplitude coefficients a_n and a_ν may be derived by substituting (2) into (1) to obtain an inhomogeneous equation which when integrated over the transverse x-dimension yields the desired equations.

$$a_n' = -\kappa_{n\nu}\, a_\nu \tag{5}$$

$$a_\nu' = \kappa_{\nu n}\, a_n, \tag{6}$$

where the coupling constants are given by

$$\kappa_{n\nu} = \frac{k^2}{12\beta_n} \langle\Delta n\rangle_{n\nu}\, e^{-i\phi_{n\nu}z} \tag{7}$$

$$\kappa_{\nu n} = \frac{k^2}{12\beta_\nu} \langle\Delta n\rangle_{\nu n}\, e^{i\phi_{\nu n}z}. \tag{8}$$

The phase constant $\phi_{n\nu}$ in (7) and (8) is

$$\phi_{n\nu} = \beta_n + \beta_\nu - K \tag{9}$$

where β is the longitudinal propagation constant in the z-direction, k is the free space wavenumber, and the wavelength of the perturbation is given by $\Lambda = 2\pi/K$.

The dominant characteristic of the modal coupling constant κ is the spatial overlap integral $\langle\Delta n\rangle$ defined as

$$\langle\Delta n\rangle_{n\nu} = \int_{-\infty}^{\infty} E_n^*(x)\; 2n\Delta n(x)\; E_\nu(x)\, dx \tag{10}$$

which requires a specification of the modal fields entering into the backward coupling process. It is evident, for example, that if $E_n = E_\nu$ in (10), then by the imposed orthogonality condition

$$\int_{-\infty}^{\infty} E_n^*(x)\, E_\nu(x)\, dx = \delta_{\nu n} \tag{11}$$

(Δn) is maximized so that the coupling can be strongest for backward diffraction between two identical modes. For coupling between different transverse modes (10) is generally much smaller so that larger perturbations need be applied to obtain reasonable coupling constants.

2. Waveguide Eigenfunctions

Before carrying out some coupled mode solutions, we review the characteristics of the propagating modes in thin-films. Appendix B reviews the propagation characteristics of asymmetrical thin-film waveguides. However, for the purposes of simplification of the mathematics for the real case where dielectrics are used for the substrates we replace the substrates by perfect conductors so that the resulting bifurcated guide is simply a thin dielectric layer on one wall of a parallel conducting-plate transmission line as shown in Figure 6.

Electromagnetically, this geometry closely resembles the actual cavity and feedback waveguide configuration illustrated in Figure 5. The cavity modes are

$$E_\nu = \begin{cases} A_3 \sin u_{3\nu}(x-t_2) & 0 \le x \le t_2 \\ A_2 \sin u_{2\nu}(x+t_1) & -t_1 \le x \le 0. \end{cases} \tag{12}$$

where the u's are transverse propagation constants satisfying the relation

$$u_{n\nu}^2 + \beta_\nu^2 = k_n^2, \qquad n = 2,3. \tag{13}$$

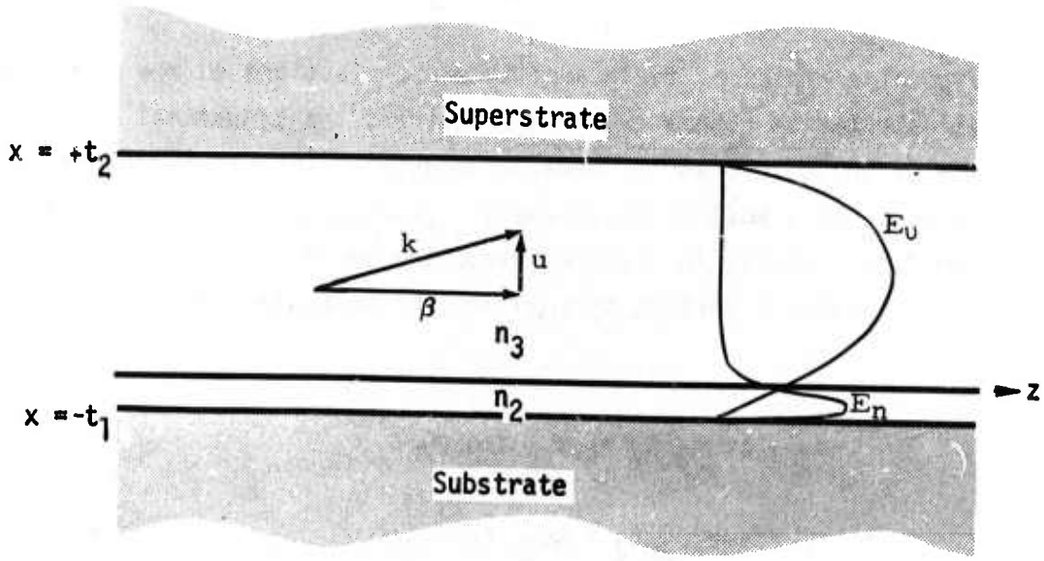

Figure 6. The Bifurcated Parallel Plate Waveguide Cavity Showing Lowest Order Cavity and Film Modes E_ν, E_n.

The cavity modes comprise a discrete set for which the longitudinal propagation constants satisfy

$$0 \leq \beta_\nu \leq k_3. \tag{14}$$

The modes primarily confined to the thin-film waveguide have the form

$$E_n = \begin{cases} B_3 \sinh u_{3n}(x - t_2) & 0 \leq x \leq t_2 \\ B_2 \sin u_{2n}(x + t_1) & -t_1 \leq x \leq 0 \end{cases} \tag{15}$$

where

$$k_3 \leq \beta_n \leq k_2 \tag{16}$$

and

$$\begin{aligned} u_{3n}^2 + k_3^2 &= \beta_n^2 \\ u_{2n}^2 + \beta_n^2 &= k_2^2 \end{aligned} \tag{17}$$

Typical examples of field amplitude distributions of the modes are illustrated in Figure 6. As required, the tangential electric fields go to zero at the metal boundaries. The psuedo-guided modes E_n have most of their energy confined to the waveguided and decay quickly in amplitude into the cavity region. Eigenvalue equations derived by matching the tangential field components at x = 0 are

$$u_{2\nu} \tan u_{3\nu} t_2 = -u_{3\nu} \tan u_{2\nu} t_1 \tag{18}$$

$$u_{2n} \tanh u_{3n} t_2 = -u_{3n} \tan u_{2n} t_1 . \tag{19}$$

If t_2 is allowed to increase without limit $t_2 \to \infty$ in (19), we obtain

$$u_{2n} = -u_{3n} \tan u_{2n} t_1 \tag{20}$$

which is the eigenvalue equation for the dielectric slab whose solutions are well known.

Normalization of the modes in (12) and (15) with respect to the relation

$$\int_{-t_1}^{t_2} E_\nu^* (x) E_\mu (x) dx = \delta_{\nu\mu} \tag{21}$$

where $\delta_{\nu\mu}$ is the Kronecker delta, gives the relations between the coefficients

$$A_3 = -A_2 \frac{\sin u_{2\nu} t_1}{\sin u_{3\nu} t_2} \tag{22}$$

$$A_2 = \frac{1}{\sqrt{2}} \left[\frac{(\sin u_{2\nu} t_1)^2}{\sin u_{3\nu} t_2} \; t_2 (1 - \operatorname{sinc} 2u_{3\nu} t_2) + t_1 (1 - \operatorname{sinc} 2u_{2\nu} t_1) \right]^{-\frac{1}{2}} \tag{23}$$

$$B_3 = B_2 \frac{\sin u_{2n} t_1}{\sinh u_{3u} t_2} \tag{24}$$

$$B_2 = \frac{1}{\sqrt{2}} \left[\frac{(\sin u_{2n} t_1)}{\sinh u_{3n} t_2} \frac{(\sinh 2u_{3n} t_2 - t_2)}{2u_{3n}} + t_1 - \frac{\sin 2u_{2n} t_1}{2u_{2n}} \right]^{-\frac{1}{2}}. \tag{25}$$

3. Coupled Mode Solutions for the Bifurcated Cavity

In this section we describe backward-Bragg-diffraction coupling between the modes E_n and E_ν on structure in Figure 6 using coupled mode theory. For simplicity, the waveguide perturbation is a periodic variation of the refractive index in the region $z \geq 0$ according to

$$\Delta n(x,z) = \begin{cases} \Delta n_2 \cos Kz & -t_1 \leq x \leq 0 \\ 0 & 0 \leq x \leq t_2 . \end{cases} \tag{26}$$

If a modulation of the film thickness, Δt, is being considered, the effective perturbation may be obtained to a rough approximation by

$$\Delta n_t \approx \frac{1}{k} \frac{d\beta_n}{dt} \Delta t \tag{27}$$

although more exact derivations have been carried out by Marcuse.

We recall that (2) expresses coupling over all modes of the spectrum. Generally we wish to compute the interchange of energy if only two modes enter into the coupling process. However, because of the small mode spacing in β_ν mode competition effects occur. It may be shown, however, that as long as the coupling length required to transfer most of the power from a film mode to a cavity mode is much longer than the transverse cavity dimension, a two-mode coupling process may be used to accurately describe the fields in the cavity region.

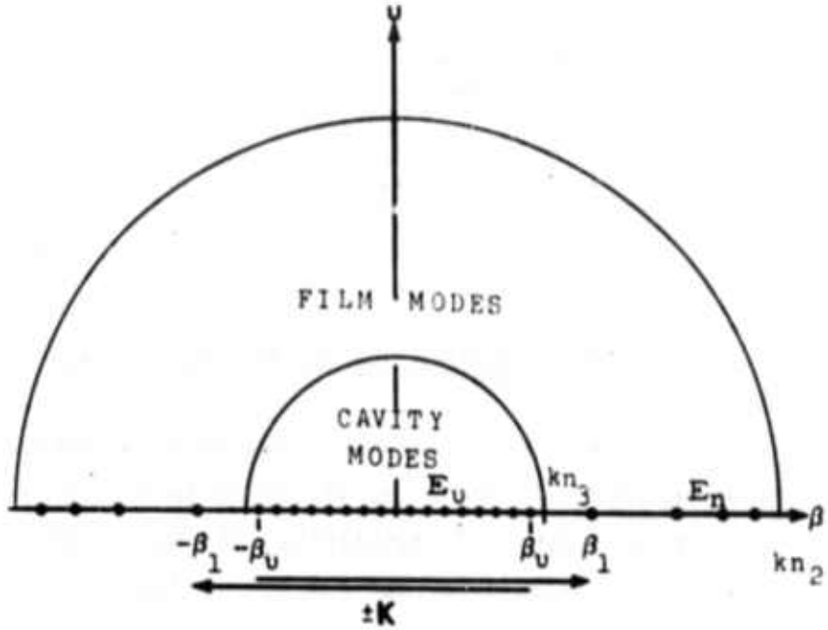

Figure 7. Mode diagram showing spectrum of discrete film and cavity modes of the bifurcated cavity.

Figure 7 illustrates the total spectrum of modes on the structure having two discrete sets of propagation constants corresponding to (14) and (16). The grating couples those modes for which

$$\beta_n + \beta_\nu = K. \tag{28}$$

Using the bounding relations (14) and (16) and the approximations $\beta_n \approx kn_2$ $\beta_\nu \approx kn_3$ (23) requires that the grating period be

$$\Lambda \gtrsim \frac{\lambda}{n_2 + n_3} \tag{29}$$

where n_2 and n_3 are the refractive indices of the film and plasma region. For $\lambda = 10.6\mu$ and a ZnSe film (29) shows that $\Lambda \gtrsim 3.1\mu$. As may be observed from the diagram, the number of cavity modes is generally large because the dimensions of the cavity are large compared to the optical wavelength . Since coupling between only one guided mode and one cavity mode is desired to avoid mode competition effects, the film should be a single mode waveguide. In addition, the grating periodicity must be small enough so that no coupling between forward and backward cavity modes can occur.

To derive the coupling constants between forward going guided modes and backward going cavity modes, we assume that a guided mode a_n is incident from the left onto the semi-infinite periodically modulated waveguide filling the half space $z \geq 0$. The cavity mode a_ν is cumulatively generated in the interaction region $0 \leq z \leq L$ and then travels back in the negative z-direction. Writing the solution to (5) and (6) in the general form

$$a_{n,\nu}(z) = A_{1_{n,\nu}} e^{-\kappa z} + B_{1_{n,\nu}} e^{-\kappa z} \tag{30}$$

and using the boundary conditions on the mode amplitudes at z=0 and L

$$a_n(0) = 1 \qquad a_\nu(L) = 0 \tag{31}$$

we find the complete solution to be

$$a_n(z) = \frac{\cosh \kappa(z-L)}{\cosh \kappa L} \tag{32}$$

$$a_\nu(z) = -i\left(\frac{\beta_n}{\beta_\nu}\right) \frac{\sinh \kappa(z-L)}{\cosh \kappa L} \tag{33}$$

where L is the length of the interaction region and the coupling constant is given by

$$\kappa = k^2 \langle \Delta n \rangle_{n\nu} / 2(\beta_n \beta_\nu)^{1/2} . \tag{34}$$

It is worthwhile to note that power is conserved as required since the sum of the reflected and transmitted powers

$$P_t = \frac{\beta_n}{\omega_\mu} \left| a_n (L) \right|^2 + \frac{\beta_\nu}{\omega_\mu} \left| a_\nu(0) \right|^2 = \frac{\beta_n}{\omega_\mu} \tag{35}$$

equals the power incident on the grating. Since the ratio of reflected to incident power at $z=0$ is

$$\frac{\beta_\nu [a_\nu(0)]^2}{\beta_n [a_n(0)]^2} = \tanh^2 \kappa L \tag{36}$$

the interaction length required for 99% coupling to the backward travelling mode results when $\kappa L \cong 3$.

The quantity $\langle \Delta n \rangle_{n\nu}$ in (34) commonly referred to as the overlap integral may be computed from (26) and (11) and the expression for the eigenfunctions in (12) and (15), where the perturbation is assumed to be sinusoidal. This results in

$$\langle \Delta n \rangle_{n\nu} = \frac{n_2 \Delta n_2}{(u_{2\nu}^2 - u_{2n}^2)} \frac{(u_{2n} \sin u_{2\nu} t_1 \cos u_{2n} t_1 - u_{2\nu} \sin u_{2n} t_1 \cos u_{2\nu} t_1)}{2A_2 3_2} \tag{37}$$

which may be simplified by utilizing several assumptions to give an approximate value of $\langle \Delta n \rangle_{n\nu}$. Using the approximations

$$u_{3\nu}(t_1 + t_2) \approx \nu\pi \qquad \nu = 1, 2, 3, \ldots\ldots \tag{38}$$

$$u_{2n} t_1 \approx \pi/2$$

we may derive

$$\frac{\langle \Delta n \rangle_{n\nu}}{\Delta n_2} = \frac{n_2 u_{3n} u_{2n} u_{3\nu} (1/u_{3n} + t_1)^{\frac{1}{2}}}{(\beta_n^2 - \beta_\nu^2) t_2^{\frac{1}{2}} (n_2^2 - n_3^2)^{\frac{1}{2}}} \tag{39}$$

The approximations in (38) are justified if the film thickness is much less than the cavity dimension $t_1 \ll t_2$ and if the TE_1 guided mode is near its cutoff, respectively.

The coupling expressed in (34) and (39) is plotted in Figure 8 as a function of the normalized propagation constant of the film-guided mode a_n for a particular geometry. The curves indicate the relative coupling constant between the TE_1 mode of the grounded slab and νth order cavity mode, and dotted lines connect points of constant grating periodicity Λ. The general characteristics of the curves indicate that coupling is strongest for the condition when the guided mode approaches cutoff $\beta_n \to kn_3$ as is expected, since the evanescent portion of the film mode then extends deeply into the gas cavity. Although the approximations (35) used to derive the curves becomes progressively less accurate for high values of ν we may nevertheless use the curves in this region to observe the behavior of the coupling. It may be noted that higher order ν-modes couple more efficiently to the lowest order n-modes. In practice, film thicknesses t_1 for which the a_n mode is reasonably far from cutoff will in general optimize the backward coupling and propagation losses in the feedback waveguide.

An example of the grating length required to reflect 99% of the power from the TE_1 mode to the oppositely travelling cavity mode $\nu = 2$ at $\beta_n/k = 1.6$ may be obtained from the curves and (3) and (36) to be $L = 5.6$ mm for $\Delta n = .01$ and $\lambda = 10.6$. In order to reduce losses resulting from scattering due to imperfect grating edges, it may be desirable to lengthen the grating to 2.24cm and use $\Delta n = .0025$.

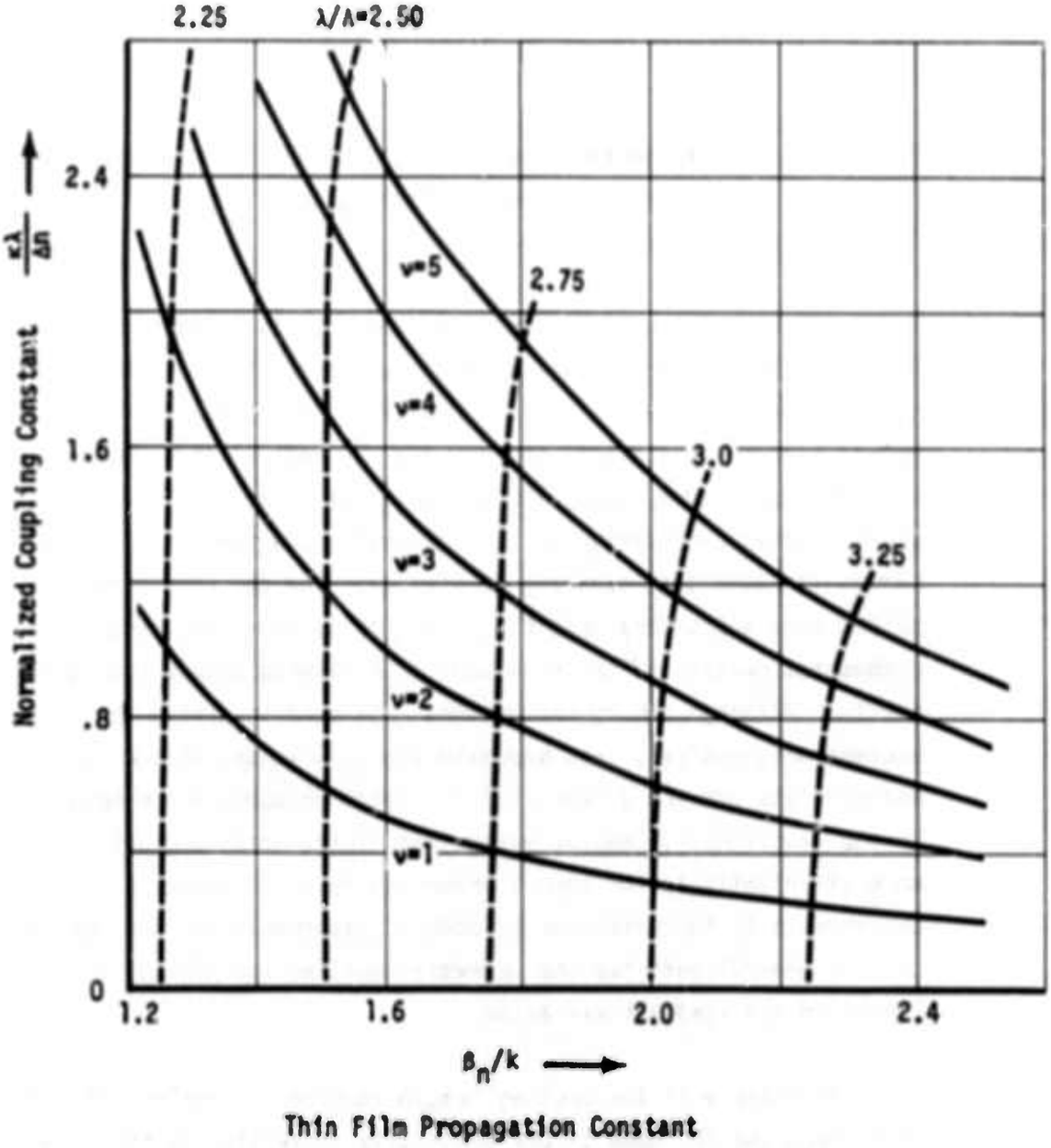

Figure 8. Normalized coupling constant betwen the TE, mode of the grounded dielectric slab a_n and the vth cavity mode a_v for n_3=3.5, n_1=1.0 and t_2=10λ. Dotted lines indicate curves of constant λ/Λ.

Figure 9 illustrates pictorially the coupling process between the incident guided mode a_n and the reflected cavity mode a_ν in the bifurcated guide of Figure 6. It may be observed that both of the mode amplitudes decay into the interaction region, but that the incident mode is never completely reflected unless the interaction length is very long.

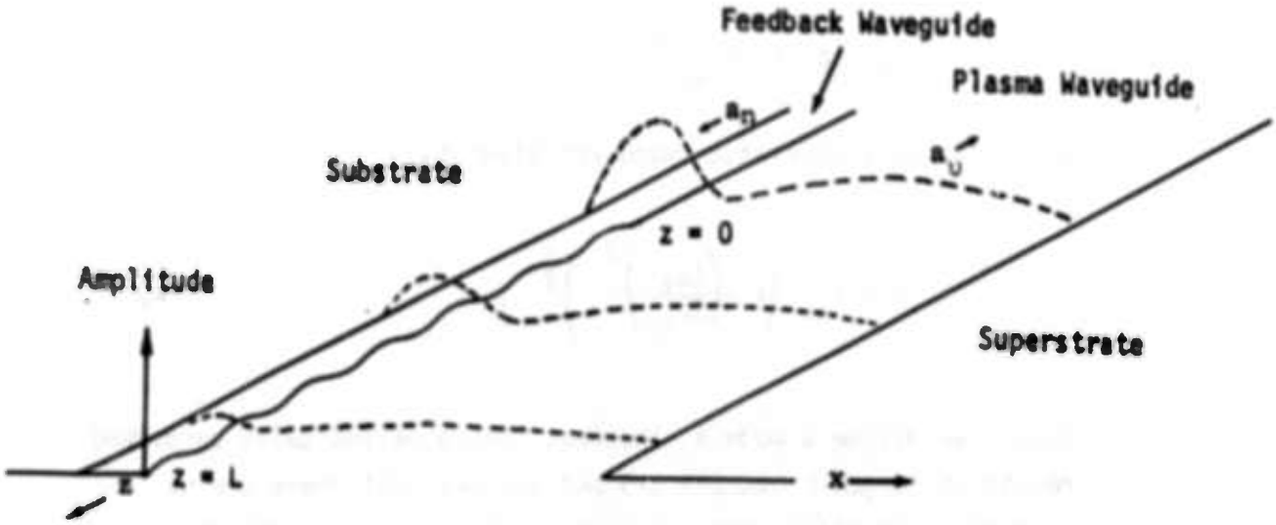

Figure 9. Illustration of the tangential electric field intensity in the interaction region due to backward coupling of modes a_n and a_ν.

4. Complex Reflection Coefficients of DFB Structures

For the purposes of describing the phase and amplitude relationships between incident and reflected waves due to distributed feedback coupling when the Bragg condition is not satisfied we return to the general solution of the coupled mode equations (5) and (6) when the coupling constants in (7) and (8) vary in phase along with the z-direction. A knowledge of these characteristics will be helpful in analyzing distributed feedback laser properties in a later section. Therefore, if phase matching is not satisfied; i.e.,

$\phi_{n\nu} \neq 0$, then decoupling the coupled mode equations (5) and (6) results in the second order differential equations

$$a_n'' - i\phi_{n\nu} a_n' - \kappa_{n\nu}^2 a_n = 0$$
$$a_\nu'' - i\phi_{\nu n} a_\nu' - \kappa_{\nu n}^2 a_\nu = 0 \tag{40}$$

having the general solution

$$a_{n,\nu}(z) = (A_{n,\nu} e^{\gamma z} + B_{n,\nu} e^{-\gamma z}) e^{\frac{i\phi_{n\nu} z}{2}} \tag{41}$$

where the characteristic roots are given by

$$\gamma = \kappa_{n\nu} \left(1 - \left(\frac{\phi_{n\nu}}{2\kappa_{n\nu}}\right)^2\right)^{\frac{1}{2}} . \tag{42}$$

Again, we assume a mode a_n incident onto a periodically perturbed region of length L between z=0 and z=L, and that there are no variations in either the x or y axes of the mode amplitudes. The boundary conditions that the incident mode amplitude be unity at z=0, and the reflected mode amplitude be zero at z=L (no reflected waves generated for z>L) give the solutions

$$a_n(z) = e^{\frac{i\phi_{n\nu} z}{2}} \left[\frac{2\gamma \cosh\gamma(z-L) - i\phi_{n\nu} \sinh\gamma(z-L)}{2\gamma \cosh\gamma L + i\phi_{n\nu} \sinh \gamma L}\right] \tag{43}$$

$$a_\nu(z) = e^{\frac{i\phi_{n\nu} z}{2} - \frac{i\pi}{2}} \left(\frac{\beta_n}{\beta_\nu}\right)^{\frac{1}{2}} \left[\frac{2\kappa_{n\nu} \sinh \gamma(z-L)}{2\gamma \cosh \gamma L - i\phi_{n\nu} \sinh\gamma L}\right]. \tag{44}$$

At the edge of the interaction region z=0, the incident and reflected modes are related by the complex reflection coefficient $r = \rho e^{i\theta}$ where the amplitude is

$$\rho = \frac{[a_\nu(0)]}{[a_n(0)]} = \left[\frac{\beta_n}{\beta_\nu} \frac{\sinh^2 \gamma L}{\cosh^2 \gamma L - (\phi_{n\nu}/2\kappa_{n\nu})^2}\right]^{\frac{1}{2}} \tag{45}$$

and the difference in phase given by

$$\theta = \tan^{-1}\left(\frac{\phi_{n\nu}}{2\gamma} \tanh \gamma L\right) + \pi/2. \tag{46}$$

We may consider three simplifying cases of (45) and (46) which differ in the value of the "detuning parameter" $\phi_{n\nu}/2\kappa_{n\nu}$.

Case (i) $\phi_{n\nu} \ll 2\kappa_{n\nu}$. This corresponds to the region near the Bragg condition for the incident wave and the complex reflection coefficient has the form

$$r = \tanh \kappa_{n\nu} L \exp\left(i \tan^{-1}\left(\frac{\phi_{n\nu}}{2} \tanh \kappa_{n\nu} L\right) + i\pi/2\right) \tag{47}$$

where $\beta_n = \beta_\nu$ has been assumed.

Case (ii) $\phi_{n\nu} = 2\kappa_{n\nu}$. At this point, the two waves are "critically" coupled, and the mode amplitudes have the simple forms

$$a_n \approx \frac{2 - i\phi_{n\nu}(z-L)}{2 + i\phi_{n\nu} L} e^{\frac{i\phi_{n\nu} z}{2}} \tag{48}$$

$$a_\nu \approx \left(\frac{\beta_n}{\beta_\nu}\right)^{\frac{1}{2}} \frac{2(z-L)\,\kappa_{n\nu}}{2 - i\phi_{n\nu} L} e^{\frac{i\phi_{n\nu} z + i\pi/2}{2}}, \tag{49}$$

and the reflection coefficient is

$$r = \frac{\kappa_{n\nu} L}{(1 + \kappa_{n\nu}^2 L^2)^{\frac{1}{2}}} \exp\left(i \tan^{-1} \frac{\phi_{n\nu} L}{2} + i\pi/2\right). \tag{50}$$

Case (iii) $\phi_{n\nu} \gg 2\kappa_{n\nu}$. In this region, very weak coupling occurs and the reflection coefficient has the well known sin x/x behavior[30] according to

$$r = \frac{\kappa_{n\nu} L}{\sqrt{2}} \operatorname{sinc} \frac{\phi_{n\nu} L}{2} e^{i\left(\frac{\phi_{n\nu} L}{2} + \frac{\pi}{2}\right)}. \tag{51}$$

Typical longitudinal behaviors of the coupled-mode amplitudes with distance into the interaction region are illustrated in Figure 10 for the three ranges of the detuning parameter in cases (i) - (iii).

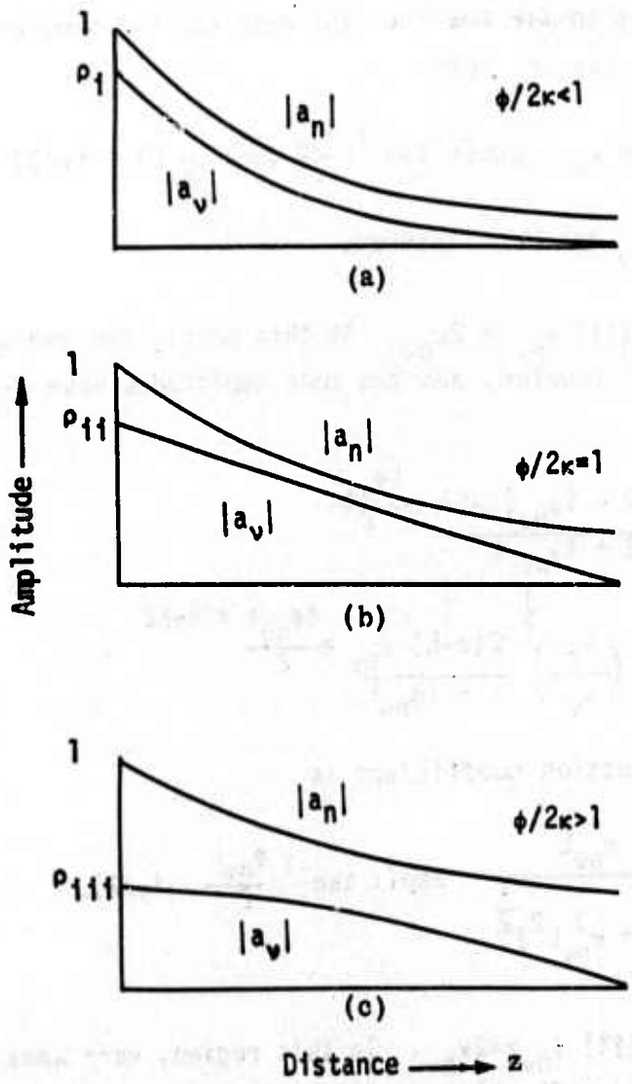

Figure 10. Typical longitudinal mode amplitude variations with distance into the interaction region of length L for (a) strong reflection near the Bragg condition, (b) critical coupling, (c) weak coupling far away from the Bragg condition.

It may be observed from (47), (50), and (51) that the phase of the reflected wave varies nonlinearly with the length of the interaction region unless the detuning is sufficiently far away from the Bragg condition. Figure 11 illustrates the magnitude and phase of reflection coefficients for several values of the coupling parameter $\kappa_{n\nu}L$. Since the curves are symmetrical about the Bragg frequency $\phi_{n\nu} = 0$, only half of the spectrum is shown. For $\kappa L = 3$, the peak reflectivity at the Bragg condition is 99% and remains relatively constant up to a detuning parameter of $\phi/2\kappa \approx 1$ and then begins to decrease more rapidly. For low gain active media such as CO_2 gas relatively high reflection coefficients would be required so that operation must usually be restricted to a detuning of less than this value. The bandwidth B_c between half-power points may be derived from (9) by noting that

$$(n_2 + n_3)\frac{2\pi}{\lambda} \cong \phi_{n\nu} + K \tag{52}$$

where the mode propagation constants have been approximated by the refractive indices of the cavity and feedback waveguide as in (29). Hence, to a good approximation

$$B_c = 2(f_c - f_o) = \frac{2c(\phi/2\kappa)_c}{\pi(n_2 + n_3)}\kappa \tag{53}$$

where $(\phi/2\kappa)_c$ is the value of the detuning parameter at the half-power points. Figure 12 illustrates both the peak reflectivity of a grating structure at the Bragg frequency and the normalized bandwidth (53) as a function of the coupling parameter κL. It may be observed that for small coupling where $\kappa L \lesssim 1$, the bandwidth changes dramatically with L if κ is kept constant, whereas for large coupling value $\kappa L > 3$, only a small change in bandwidth occurs with increasing L. An example of the bandwidth for a grating structure in a thin film of GaAs $n_2 = 3.3$ at $\lambda = 10.6\mu$ for which coupling of strength $\kappa L = 3$ occurs between a thin film mode and a CO_2 gas cavity $n_3 = 1.0$ as in Section II-B may be obtained from Figure 12 and (53) to be

$$B_c = .57\,\frac{c}{L} \tag{54}$$

or about 3.4 GHz if L = 5 cm.

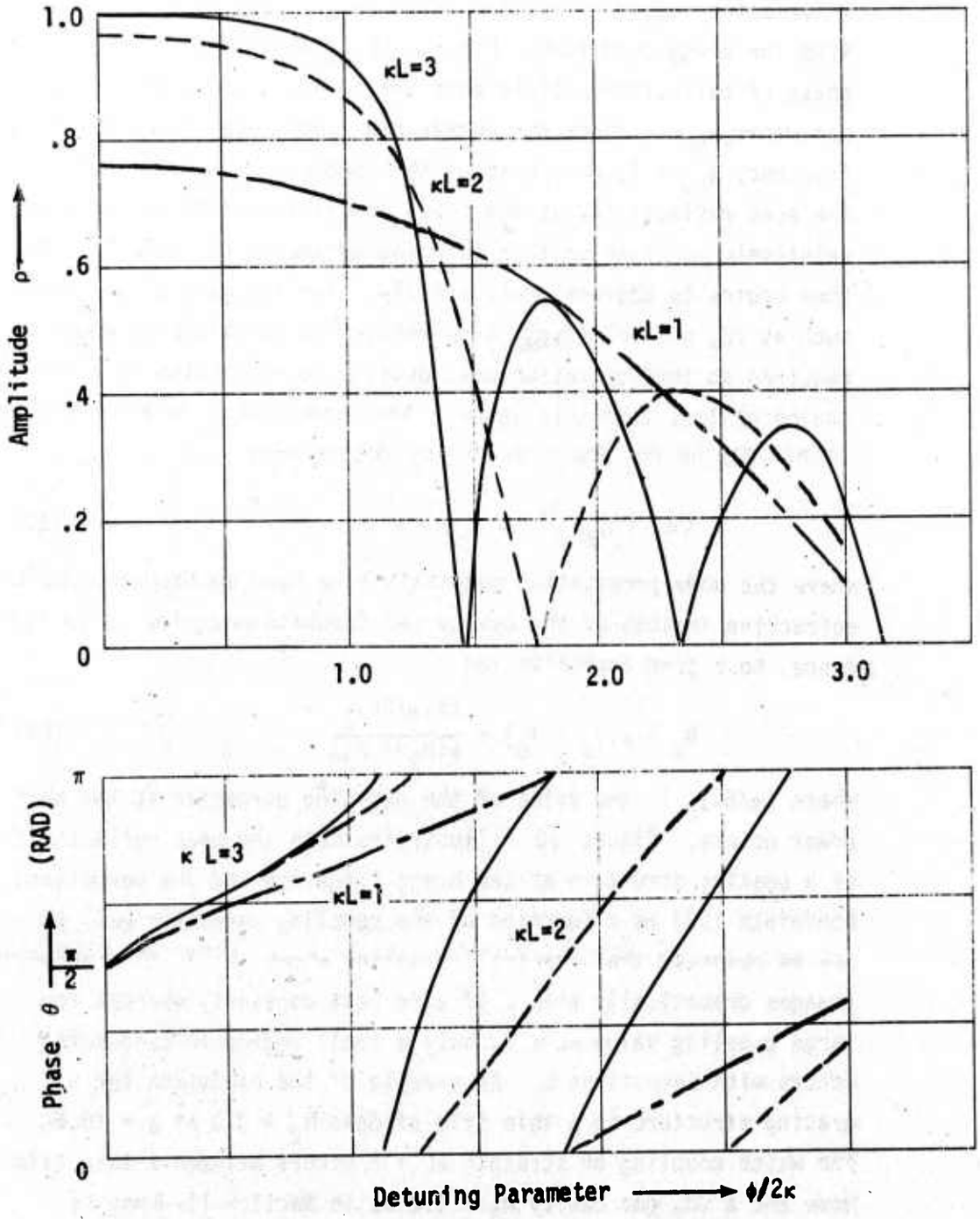

Figure 11. Phase and amplitude relative to the incident mode of the mode coupled in the backward direction by a periodic structure as a function of the detuning from the Bragg condition and coupling parameter L.

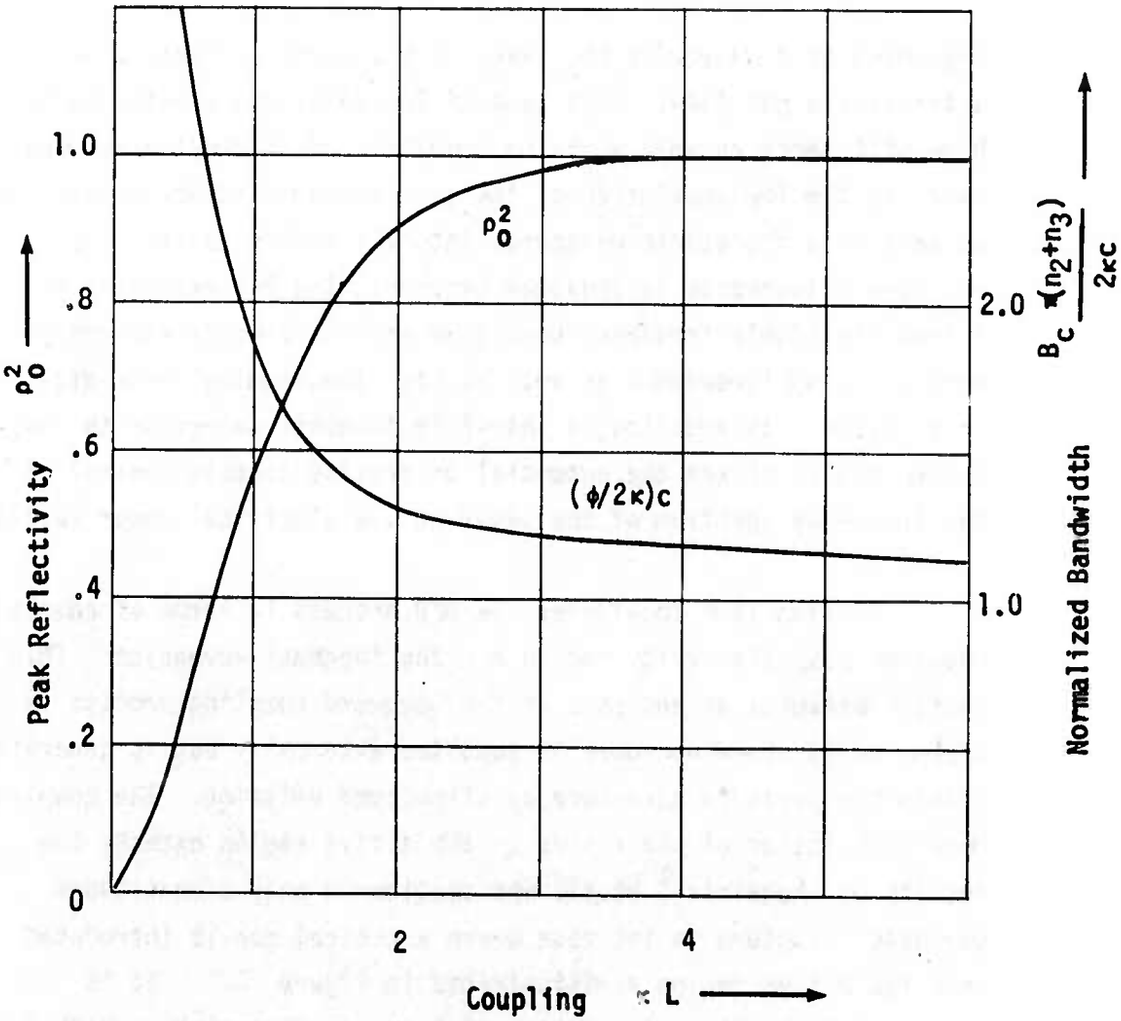

Figure 12. Peak power reflectivity ρ_o^2 at the Bragg condition and normalized bandwidth $(\phi/2\kappa)_c$ as a function of the coupling parameter κL for backward-wave coupling.

C. DISTRIBUTED FEEDBACK CO_2 LASERS

1. The Concept of Laser Miniaturization

Recent advances in CO_2 waveguide gas lasers[3,6-8] providing greatly increased volumetric power outputs by virtue of plasma confinement to an optical waveguide has led to an interest in

implementing a waveguide CO_2 laser into a planar structure having a transverse gas flow. This type of CO_2 laser has a potentially high efficiency as well as being compact. Of interest here, however, is the implementation of the distributed feedback mechanism as well as a dielectric-waveguide into the active cavity. As has been illustrated in previous sections, the DFB mechanism is inherently highly frequency-sensitive and can provide extremely narrow lasing linewidths as well as high longitudinal mode discrimination. In addition, a thin-film feedback waveguide in the active cavity offers the potential of precise tunable control of the frequency spectrum of the laser at low electrical power levels.

Section II-B considered the DFB process in terms of coupled modes of both the cavity region and the feedback waveguide. This section presents an analysis of the backward coupling process in active media where no power is supplied externally but is generated within the periodic structure by stimulated emission. The coupled mode description of the fields in the active region extends the results of Kogelnik[19], et.al. who considered only a continuous periodic structure to the case where a central gap is introduced into the active region as illustrated in Figure 5. It is important that some optimization of laser characteristics with respect to threshold gain and lasing spectrum can be achieved in distributed hetero-feedback DHFB lasers with longitudinally-varying feedback.

2. Resonance Modes in Periodic Active Media

For simplicity, we consider the one-dimensional periodic structure shown in Figure 13(a) on which the fields may be described by coupled modes. The natural modes of oscillation are

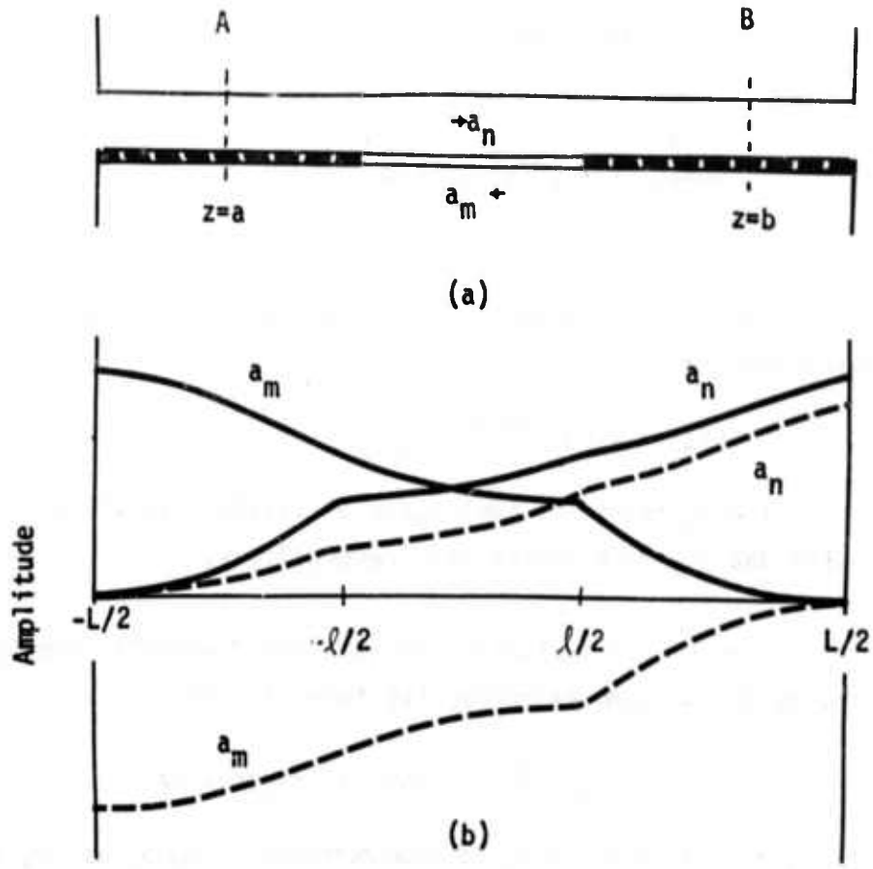

Figure 13(a). The configuration of the semi-continuous distributed feedback laser for which an integral number of central fingers have been removed.
(b). A typical longitudinal-mode amplitude distribution at threshold for symmetric and anti-symmetric (shown dotted) field distributions.

determined from the field solutions which satisfy the wave equation and boundary conditions in each of the regions of the cavity. This theory can only predict the lasing modes at threshold and is not valid if the net gain is non-zero. Figure 13(b) illustrates the typical mode amplitudes in the active region, where because no external energy is being applied, the modes carrying power toward the center of the active region must go to zero at the boundaries $z = \pm L/2$ as shown.

The solutions to the waves in the entire laser cavity satisfy the wave equation

$$\frac{\partial^2}{\partial z^2} E + k_0^2 n^2 E = 0 \tag{55}$$

where the total TE wave vector E_y may be represented by the coupled mode pair

$$E(z) = a_n(z) e^{i\beta_n z} + a_m(z) e^{-i\beta_m z} \tag{56}$$

where a_n and a_m represent amplitudes of fields travelling in the positive and negative z-direction respectively.

Assuming a distribution of gain and dielectric constant according to the complex refractive index in (55)

$$n(z) = (n_r + in_i) - (\Delta n_r + i\Delta n_i)\cos Kz \tag{57}$$

where n_i is the gain and n_r is the refractive index, we may show that the complex wavenumber $k = k_0 n$ may be approximated using the conditions

$$n_i, \Delta n_r << n_r. \tag{58}$$

to give

$$k^2 = k_0^2(n_r^2 + i2n_r n_i) + 2k_0^2 n_r(\Delta n_r + i\Delta n_i) \cos Kz. \tag{59}$$

In the present analysis, no gain modulation is considered so that $\Delta n_i = 0$. Substituting (56) and (59) into (55) gives the coupled equations

$$\begin{aligned} a_n' + k_c a_n &= i\xi a_m \\ -a_m' + k_c a_m &= i\xi a_n \end{aligned} \tag{60}$$

where

$$k_c = k_o\left[n_1 - i\left(1 - \frac{\omega_o}{\omega}\right)\right] \tag{61}$$

$$\xi = \frac{k_o}{2}\,\Delta n_r \tag{62}$$

and $(1-\frac{\omega_o}{\omega})$ represents the detuning from the Bragg frequency ω_o.

The solutions to (60) for fields in the periodically varying regions have the form $e^{\pm\gamma_a z}$ where

$$\gamma_a^2 = k_c^2 + \xi^2. \tag{63}$$

In the region without perturbation $-\ell/2 \leq z \leq \ell/2$, (55), $\xi = 0$ in (55) and (60) has solutions of the form $e^{\pm\gamma_b z}$ where

$$\gamma_b = k_c \tag{64}$$

leading to exponentially growing waves which are uncoupled.

The subscript notation (1,2) is used to refer to solutions in the periodic and homogeneous regions of the DFB laser respectively. Since the structure is symmetrical only the righthand portion $z \leq 0$ need be considered to obtain the mode amplitudes over the entire cavity. Furthermore, the odd and even field symmetry $E(z) = \pm E(-z)$, leads to corresponding mode symmetry conditions $a_n(z) = \pm a_m(-z)$. Noting the boundary condition

$$a_{m_1}(L/2) = 0 \tag{65}$$

we take

$$a_{m_1}(z) = A \sinh\gamma_a\left(z - \frac{L}{2}\right) \qquad \ell/2 \leq z \leq L/2. \tag{66}$$

The other mode solution is determined by substituting (66) into the second differential equation of (60) to give

$$a_{n_1}(z) = -\frac{1}{\xi} A\left[-\gamma_a \cosh\gamma_a(z - \tfrac{L}{2}) + k_c \sinh\gamma_a(z - \tfrac{L}{2})\right] \qquad (67)$$

$$\ell/2 \leq z \leq L/2.$$

In the region where there is no coupling, the mode amplitudes may be within

$$\begin{aligned} a_{n_2} &= B e^{\gamma_b z} \\ a_{m_2} &= \pm B e^{-\gamma_b z} \end{aligned} \qquad 0 \leq z \leq \ell/2. \qquad (68)$$

At the boundary $z = \ell/2$, the mode functions of (66) - (68) are continuous so that

$$\begin{aligned} a_{m_1} &= a_{m_2} \\ a_{n_1} &= a_{n_2} \end{aligned} \qquad z = \ell/2. \qquad (69)$$

A division of the two equations in (69) yields the complex characteristic equation

$$-k_c \pm i\xi e^{\gamma_b \ell} = \gamma_a \coth \gamma_a(L-\ell)/2 \qquad (70)$$

which must be solved to determine the complex longitudinal mode propagation constant γ_a. The + and - signs in the eigenvalue equation hold for anti-symmetric and symmetric modes, respectively. In the limit $\ell \to 0$ where the grating is continuous over the entire cavity (70) reduces to the eigenvalue equation derived by Kogelnik.[19] This may be shown from (70) by using the identity $\coth x = \sinh^{-1} 2x + \coth 2x$, and the dispersion relation (63) to derive the equivalent

characteristic equations valid at $\ell = 0$ to be

$$k_c = -\gamma_a \coth\gamma_a L$$
$$\xi = \pm\, i\gamma_a/\sinh\gamma_a L. \tag{71}$$

The eigenvalue equations (70) and (71) have roots which are dependent upon parameters such as gain, frequency, and coupling constant as well as the gap length ℓ and yield the resonant frequencies for oscillations at threshold and the corresponding threshold gains. In general, the solutions must be determined by numerical techniques which are difficult because of the multidimensionality. In the case of low gain, such as the CO_2 system, however, (70) may be simplified to obtain some approximate solutions for the laser oscillation spectrum.

3. Laser Spectra Approximations

At very low values of gain $n_1 << \Delta n_r$, a separation of (70) into its real and imaginary parts and an expansion of the right side give the equation

$$e^{k_0 n_1 \ell} \cos k_0\left(1 - \frac{\omega_0}{\omega}\right)\ell = \pm \frac{2}{\Delta n_r}\left(1 - \frac{\omega_0}{\omega}\right) \tag{72}$$

whose solution gives the location of the first resonance above and below the Bragg frequency ω_0. Successive resonances which appear due to the multiple branches of the complex hyperbolic function in (70) are difficult to approximate but are also less important than the primary modes because they require considerably higher threshold gains. It may be observed from (72) that the DHFB laser does

not oscillate exactly at the Bragg frequency, since no solution exists at $\omega = \omega_0$. This is a result of the fact that the periodic structure has a frequency stop-band whose width is directly proportional to the magnitude of the coupling Δn_r.[19] This topic will be discussed further in a later section.

When the gap length ℓ approaches zero (72) has the first resonances spaced by

$$\omega - \omega_0 \cong \pm \frac{\Delta n_r}{2} \omega_0 \tag{73}$$

where the corresponding threshold gain is approximately

$$k_0 n_1 L = \left(\frac{\lambda}{\Delta n_r L} \right)^2. \tag{74}$$

Taking the gain to be about 2db for which $k_0 n_1 L = .23$, (74) and (73) indicate that the laser will oscillate in two primary modes symmetrically located about the Bragg frequency and separated by

$$\Delta f = 2(f - f_0) \cong 2c/L \tag{75}$$

where c is the speed of light in vacuo. This frequency difference may be compared to $\Delta f = c/2L$ for a conventional cavity of the same length. It may be observed that oscillation may be achieved at even very low gains by increasing the refractive index perturbation to a sufficiently high value which simultaneously widens the frequency difference between the first order modes. Figure 14 illustrates the mode spacing and required threshold gain as a function of the coupling strength for the low gain case. As

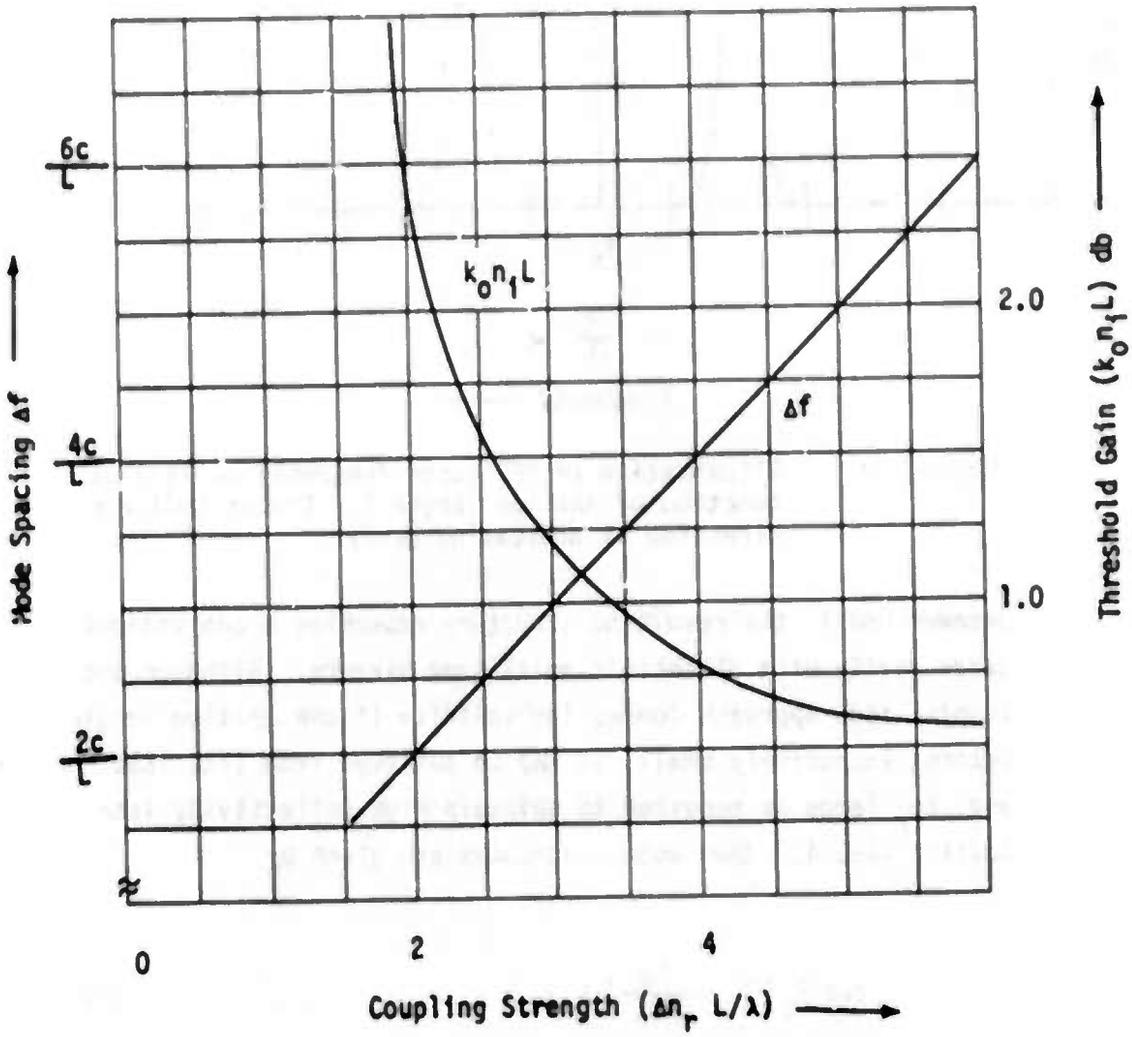

Figure 14. Approximate frequency separation between primary modes and the required threshold gain as a function of coupling in the continuous DFB laser ($\ell = 0$).

expected the threshold gain decreases as the coupling is increased, so that it is important to note that the laser power output will in principle be limited not by the distributed feedback but by scattering and absorption losses in the active cavity.

As the width of the gap ℓ is increased while maintaining the total length L constant equation (72) indicates that the first-order resonances move closer together. In particular, it is interesting to note that in the limit for which the length of the grating $(L-\ell)/2$

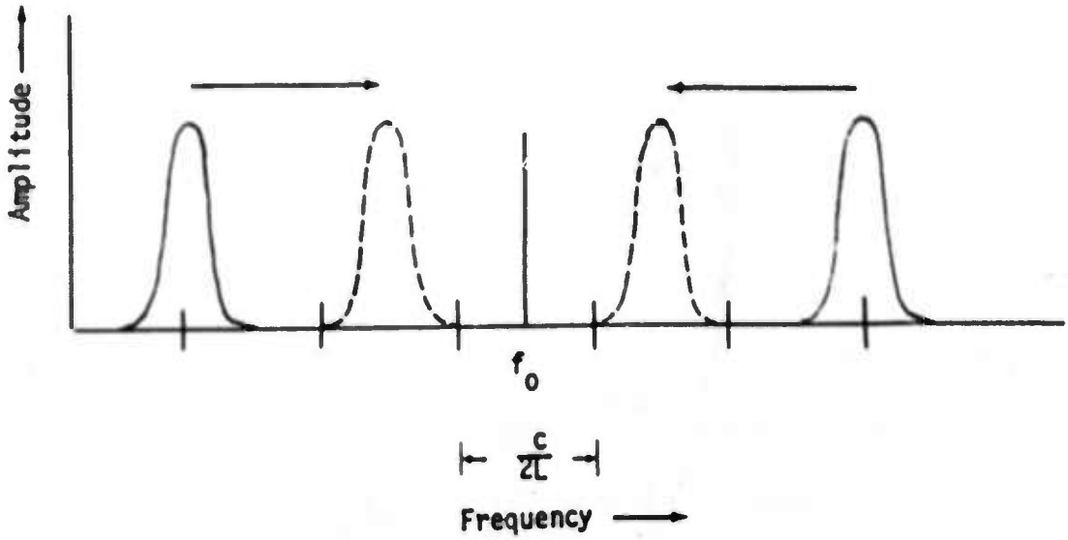

Figure 15. Illustration of DFB laser frequency pulling as a function of the gap length ℓ. Arrows indicate direction of decreasing $(L-\ell)$.

becomes small, the resulting structure resembles a conventional laser cavity with dielectric multilayer mirrors. Although the coupled mode approach looses its validity if the grating length becomes excessively small, it may be observed from (72) that for $\ell \to L$ and Δn_r large as required to maintain high reflectivity (see Section II-C-4), the mode resonances are given by

$$\cos k_0\left(1 - \frac{\omega_0}{\omega}\right) L \cong 0 \tag{76}$$

from which we have

$$f - f_0 \cong \frac{c}{2L}\left(n - \frac{1}{2}\right) \qquad n=0, \pm 1, \pm 2 \ldots \tag{77}$$

Figure 15 illustrates the frequency "pulling" of first order resonances when the gap length ℓ increases in the direction of the arrows. Varying ℓ by some fraction of the total cavity length will move the resonances between the curves indicated by solid and dashed lines. Not shown on the diagram are higher-order modes. As has been illustrated in Figure 14 this frequency-pulling

effect also occurs for a continuous gap where $\ell = 0$ when the refractive index coupling Δn_r is varied. These phenomena reveal interesting possible approaches to selective tuning of DHFB lasers by electro-optic control of the coupling strength or its longitudinal distribution in the laser.

Figure 16 shows the variation in the frequency spacing between first order modes as functions of the gap length ratio ℓ/L for several values of coupling. For zero gap length, the primary mode spacing is maximum and decreases towards c/2L as the gap lenth becomes larger. It is evident that when ℓ approaches half of the total laser length, the mode spacing is close to c/2L and does not vary appreciably with the coupling at threshold. This behavior results from the fact that as the feedback gratings become progressively shorter, very little power results from stimulated emission within the periodic structure and the gratings become passive reflectors within the cavity. It may be observed that a tuning range is possible of several times the conventional cavity mode spacing frequency or about 7 GH_z for a laser length L = 10 cm having a gain $k_0 n_1 L \approx 2$db. The use of electro-optic structures to generate the periodicities in DHFB lasers are attractive for use in electronic tuning of the laser since the frequency may be tuned without introducing a simultaneous modulation on the threshold gain, and therefore the laser power output. It was shown that the latter effect occurs for continuous DFB structures when the coupling constant Δn_r is varied.

The DFB laser of the continuous or semicontinuous type discussed here has the characteristic of not lasing exactly at the Bragg frequency in a single mode but instead lasing in two primary modes of equal strength symmetrically located about the Bragg frequency. For some applications, single mode outputs may be desired, but we

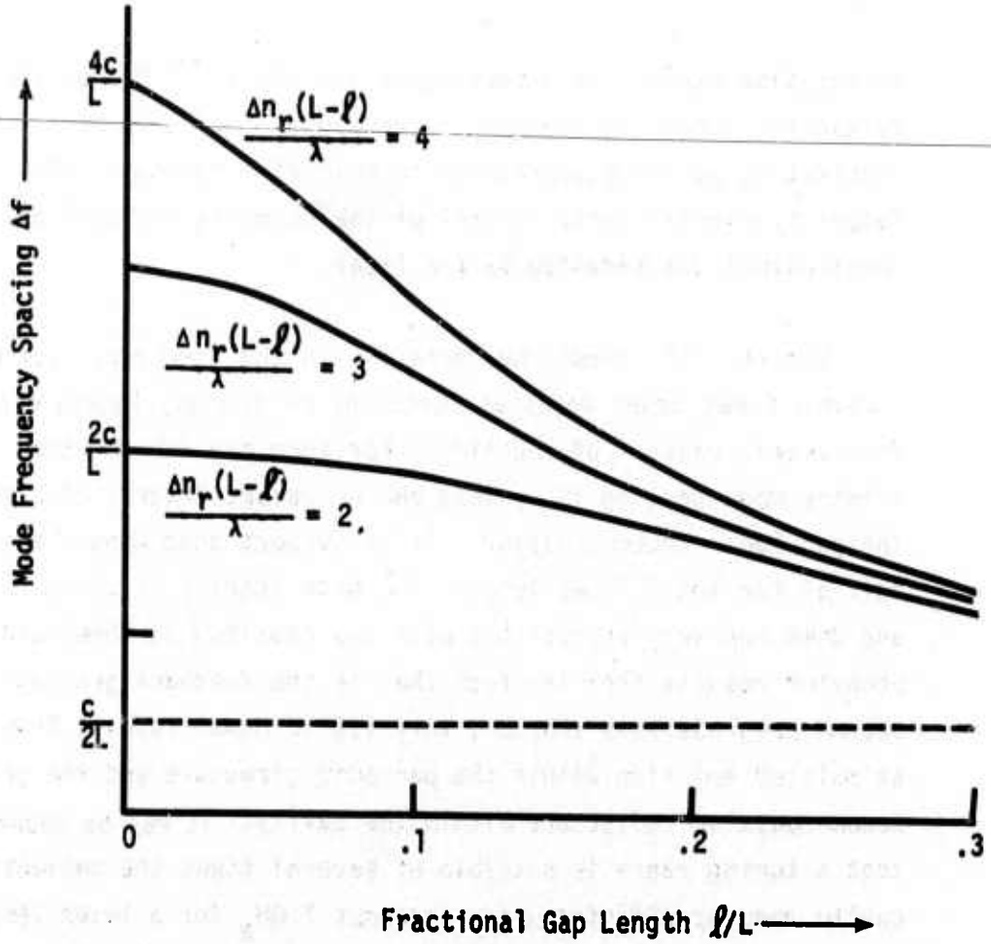

Figure 16. Frequency spacing between primary resonances of the distributed hetero-feedback laser at threshold.

first discuss these characteristics in more detail. It is well known that periodic structures have frequency stopbands in the dispersion diagram for which no unattenuated propagation through the material is possible. In the case of the DFB laser, however, the fact that oscillation does not occur at the Bragg frequency may be simply viewed as a result of a phase mismatch for any round-trip path in the periodic structure. Section II-B-4 discusses the phase characteristics of backward Bragg coupling noting that at the Bragg condition, the reflected wave is $\pi/2$ radians out of phase with the incident wave. Furthermore, this phase relationship is preserved throughout the periodic structure if the phase is measured at the boundaries such as "A" or "B" in Figure 13 between identical cells of the grating. Viewing the planes $z=a$, $z=b$ as idealized reflection points for a cavity of length $b - a$, it is clear that the lasing condition is specified by

$$\theta_b + \theta_a + 2\pi(\lambda_c^{-1} + \lambda_f^{-1})(b-a) = 2n\pi \qquad n=0,1,2 \ldots \quad (78)$$

where θ is the relative phase of the reflected wave at the respective points, and λ_c and λ_f are the wavelengths in the cavity and feedback waveguide. At the Bragg frequency, θ is $\pi/2$; and since we may take $(b-a) = m\Lambda$, $m = 0, 1, 2 \ldots$ (78) requires

$$\lambda_c^{-1} + \lambda_f^{-1} = \frac{1}{\Lambda}\left(\frac{n}{m} - \frac{1}{2m}\right) \qquad (79)$$

which is not satisfied because the integer expression in parentheses cannot be made constant. For frequencies not equal to the Bragg frequency, the phase-matching condition in (78) can be satisfied if the combined phase shift $(\theta_a + \theta_b)$ changes in a negatively linear fashion with $(b-a)$ $(\lambda_c^{-1} + \lambda_f^{-1})$. This variation in the phase at reflection with grating length may be observed from Figure 10 and it is interesting to note that oscillation will occur at only a number of discrete wavelengths.

D. EXPERIMENTAL EFFORT

1. Capillary Waveguide CO_2 Laser

During the initial effort, a series of CO_2 capillary gas lasers was constructed based upon the design of Bridges, et al[7]. This effort provides data relative to the gas discharge characteristics, optimum gas composition, operating characteristics at moderate gas pressures (100 Torr), gain and thermal characteristics. From these data and comparison with the literature, a new capillary was constructed and its operation demonstrated which employed a reduced capillary bore diameter of 0.6mm. The results of this latter extension confirms an enhanced gain due to the further confinement of the discharge. It also indicates the limitation imposed by the inhomogeneous pressure distribution due to the high pressure drop through the capillary.

The photograph of Figure 17 shows one of these lasers in operation. Standard Pyrex capillary tubing with bore diameter of 1.0mm with wall thickness of 5mm was initially employed. The thermal impedance for this large wall proved too high as evidenced by electrical punch-through. Further undulations during the drawing of the capillary proved to cause excessive losses. Two capillary plasma discharge tubes employing a 1.0mm diameter bore and a 0.6mm diameter bore were constructed using a precision-ground tubing with a wall thickness of 1.0mm for both cases. The reduced wall thickness provided a substantial improvement of the thermal stability. **Precision bore** capillary with flared ends always operated in the TEM_{00} mode. Data from this hardware has been included in Table 1.

The Fabry-Perot reflectors were fabricated from NaCl using a radius of 8cm positioned at 7.4cm from the capillary throat. For the 1mm bore diameter, these parameters minimize the losses. Semi-transparent gold films were employed for the output coupling. Measurements of the transmission, reflection and absorption were derived from insertion in a CO_2 laser beam. Fabry-Perot reflectors of 90% exhibited 8% absorption while reflectors in the 80% regime exhibited absorption of approximately 15%.

Preceding page blank

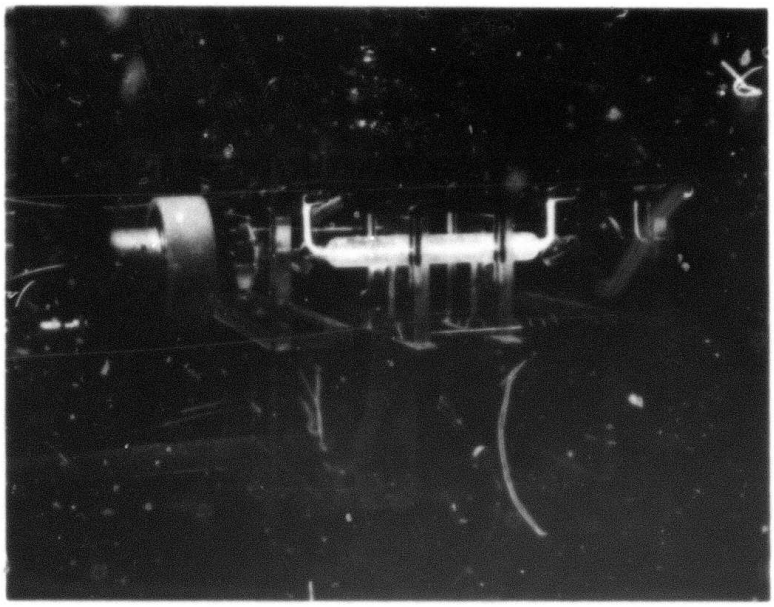

Figure 17. Six-Tenths Millimeter Bore Capillary CO_2 Laser

Further reduction of the reflectivity resulted in correspondingly increased absorption. Some evidence indicates that a proportion of absorption of gold films on NaCl is time-dependent. Using the 1mm bore capillary, a 90% reflecting Fabry-Perot, a combined gas pressure of 100 Torr at the input and the optimum current of 3.5mA, 200mW was measured on the P20 emission line. The Fabry-Perot reflectivity was not optimized and no account for the absorption is included. These experimental parameters were derived using methanol cooled to dry ice (230°K).

Using the identical Fabry-Perot reflectors and substituting the 0.6mm bore capillary laser operation was demonstrated even with the mismatch of capillary aperture to the Fabry-Perot.[32] The maximum power output measure was 120mW at 120 Torr at the input and an optimum current of 1.3mA. Noting the additional losses due to the capillary aperture mismatch to the reflector radius and the further inhomogeneous plasma discharge pressure profile, this latter result substantiates the increased gain due to the further confinement by the capillary waveguide walls. The additional losses due to aperture mismatch is 10% at each end. It, however, also dramatically increases the need for a uniform plasma discharge temperature and uniform plasma pressure throughout the active region.

The arithmetic average collision-broadened emission line width for these experiments is approximately 300MHz whereas the longitudinal Fabry-Perot mode period is 625MHz. Under these conditions, slight changes of mechanical dimensions and discharge parameters cause the capillary laser to mode-hop over a variety of initial lines in both the R and P branches.

2. CO_2 Planar Plasma Discharge

A major fraction of the experimental effort has been devoted to investigation of various means to create a continuous uniform CO_2 plasma discharge in the hollow active planar waveguide. Thus far, this effort has been unsuccessful, however, not all approaches have been adequately investigated. Several recent experiments show promise that require further effort to realize a continuous uniform plasma discharge "in progress." The transverse excitation and transverse flow art [34-41] applied to the CO_2 laser has been developed to alleviate the problems associated with the coincident longitudinal configurations. These developments have emphasized approaches to achieve high energy, high power and high volumetric efficiency. Some experiments have employed gas pressure in excess of an atmosphere and flow rates approaching the sonic level. In all cases, the volumes are of multi-centimeter dimensions. With one exception (Ref. 42), all the plasma discharges have been pulsed with a variety of techniques to ionize the gas. The effort reported herein has been confined to the continuous discharge and to chambers of submillimeter wall separation. The following exposition delineates the various experiments performed.

In all cases, the plasma discharge chamber investigated conforms to the structure illustrated in Figure 1 and 2. The waveguide region in which it is essential to produce a uniform continuous plasma has dimensions of 100 microns thickness, 3-5 mm width and 10 cm length. Transverse flow of the gas mixture and transverse excitation occurs across the 3-5 mm dimension. Two channels approximately 6 x 6 mm have been provided parallel and adjacent to the active hollow waveguide as low impedance gas channels to produce a uniform pressure in the active waveguide region.

The initial experiments employing hollow anode and cathode electrodes at the input and output ports of the substrate typically produce a diffused plasma extending throughout the side channels with a concentrated arc across the active waveguide. The location of the concentrated arc along the length is unstable. Changes of the ballast resistance in series with the power supply over a wide range does not alter the concentrated arc discharge characteristics. The concentrated arc is observed at pressures of the few Torr up to several hundred. Fractional Torr pressure produces a diffused plasma in the waveguide region having a width of a few mm, whereas the width should extend over 10 cm. Including an additive such as Xe does not alter the spatial distribution.

One of the more successful quasi-uniform discharges is illustrated in the photograph of Figure 18. A DC-excitation was employed. The distributed discharge was created by introducing surface resistance along the adjacent channels (via a pencil mark). The discharge at 30 Torr could be sustained for only a few hours before relaxing into a concentrated arc as above. This effort has been traced to sputtering in the waveguide chamber.

A series of experiments had been performed using RF-excitation at 27 MHz with a kilowatt being available. A uniform continuous discharge is formed in the adjacent channels with a concentrated arc appearing in the waveguide chamber using the anode and cathode electrodes above. Use of capacitive electrodes above the superstrate also produces a uniform continuous plasma in the adjacent chambers. However, without penetration into the waveguide chamber.

Experiments have been performed using RF-excitation drive from a K_u band-pulsed magnetron of 250 KW peak. In the high power density region and pressures of a few tens of Torr, a discharge could be produced in the waveguide chamber, however, with considerable sputtering of the glass surfaces. Increasing pressure creates a filamentary structure and eventually arcing.

Another approach investigated employs a comb cathode or anode structure composed of 25 or 50 pin electrodes, using ballast resistors in the meg-ohm range. The ballast resistors have been connected to a common bus and encapsulated in a silastic. A plan view through the substrate showing

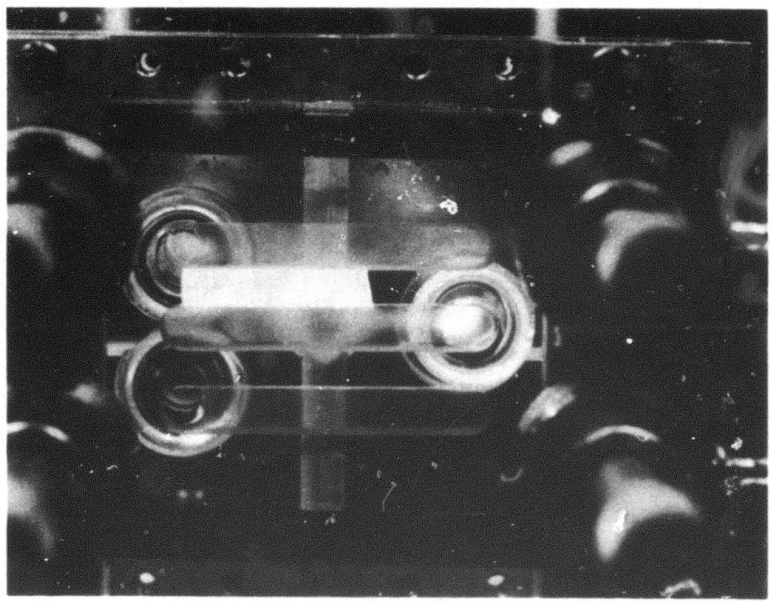

Figure 18. Plan view through substrate showing a quasi-uniform discharge 100 microns thick, 5 mm wide, 5 centimeters long at 30 Torr.

the waveguide chamber adjacent channels containing a tungsten anode wire and a comb resistor array cathode is illustrated in Figure 19. The gas flow occurs from the anode to cathode through the input and output ports at the end of the channels. Figure 20 is identical to Figure 19 using only the plasma discharge for illumination. The glow discharge is evident in the cathode chamber. Concentrated arcs sporadically occur throughout the waveguide chamber which in the figure is 9 centimeters long. The CO_2-N_2-He gas mixture pressure is approximately 30 Torr. The arcs exhibit a higher degree of concentration at pressures greater than 100 Torr. Considerable sputtering of the cathode material (Cu) occurs in a comparative short time.

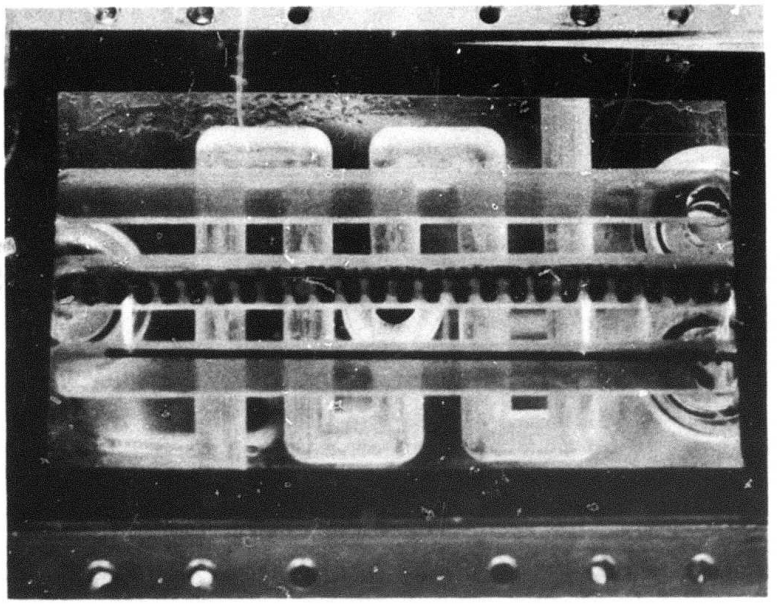

Figure 19. Plan view through substrate showing concentrated arcs between tungsten anode and comb ballast resistor cathode structure.

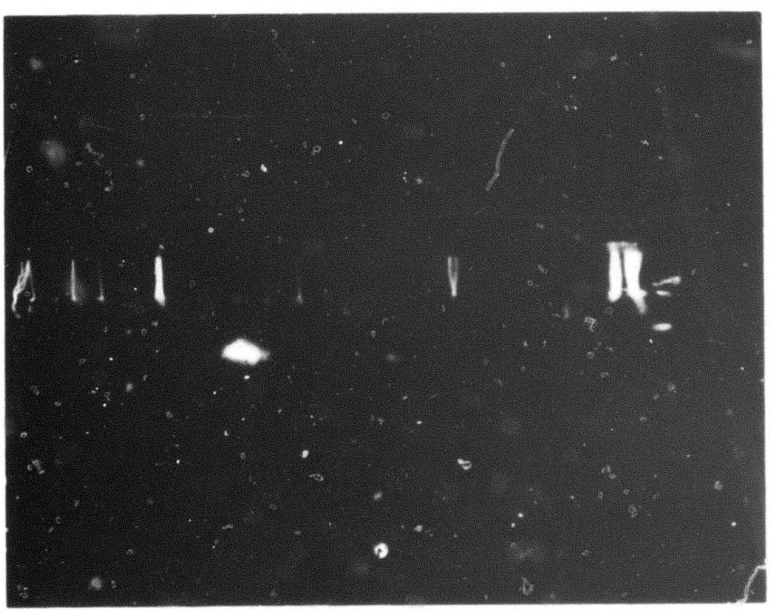

Figure 20. Same as Figure 19 showing glow discharge in the vicinity of cathode comb together with concentrated arcs.

Several approaches are being investigated to obtain a continuous uniform plasma discharge. Two strip-ribbon electrodes are deposited adjacent to the feedback waveguide grating structure positioned over the adjacent channels. RF-excitation is to be applied in this structure. In this structure the electric field is concentrated and oriented in the ~~waveguide~~ plane. Another approach being investigated employs one of these aluminum strips as the anode and a comb array of tungsten field emitters as the cathode in a DC excited discharge. This will permit adjustment of the ballast resistors external to the chamber to optimize the discharge uniformity. The array of field emitters will be aligned and terminate the edge of the waveguide chamber. The laser superstrate containing the gas manifold is being formed from polycrystalline BeO to assure a homogeneous thermal wall as one face of the hollow active waveguide. Further, it is intended that the transverse flow velocity be substantially increased such that the transit time of the gas through the discharge is made significantly less than the diffusion time of positive ions to the walls of the waveguide chamber [35]. Thus, the current and temperature distributions should depend more on the way in which the discharge is established at the upstream electrode, rather than on the transverse diffusion processes [39, 41]. This should reduce the tendency of discharge to contract into narrow arcs and should be somewhat independent of pressure. If this approach does not reduce the dominant effect of transverse diffusion processes to the walls, it will be necessary to increase the waveguide thickness which will in turn have a significant impact upon the backward wave Bragg defraction coupler design.

3. Backward Wave Bragg Diffraction Coupler

The experimental effort devoted to the production of the passive feedback waveguide and the backward wave Bragg diffraction couplers, together with techniques to produce same, are delineated in this section.

A variety of thin film passive waveguides have been produced by evaporation and RF-sputtering. Major attention has been given to ZnSe, ZnS, on glass substrates and TlBr/I on NaCl, BaF_2, and NaF substrates. Metallic mask had been used to form the passive waveguide width (3-5 mm). The dielectric waveguide thus formed is a rectangular dielectric image line struc-

ture. However, the optical field confinement is not produced by the waveguide but instead by the backward wave Bragg diffraction coupler grating. No difficulty has been encountered with the zinc compound deposits on glass substrates. The TlBr/I deposits on materials transparent at 10 microns has exhibited a deterioration with time and exposure to the atmosphere, presumably due to the fact that TlBr/I sublimes at low deposition temperatures. The use of a dielectric feedback waveguide requires the alteration of the grating period by both the film thickness and refractive index. Most of the experiments pertaining to the development of the backward wave grating coupler have not been performed on a passive feedback waveguide film, but instead have been implemented on the surface of the active gas waveguide walls (glass). This temporary expedient procedure allows the investigation of the contra-directional coupler with a grating using a fixed grating period equal to one half the CO_2 emission line wavelength.

Most of the effort has been devoted to the development of the backward wave diffraction coupler using a grating as an iterative structure. Various techniques are available to produce the iterative structure. They include (1) the periodic alteration of the dielectric waveguide cross section, (2) the periodic alteration of the dielectric refractive index by changes of the material composition and (3) by the creation of a traveling surface elastic (Rayleigh) wave. The latter is intended for tuning of the feedback waveguide. The second technique may be implemented by diffusion, ion implantation, ion exchange, alloying, etc. These techniques in general create a comparatively small perturbation, thus requiring a long iterative structure to affect efficient coupling.

The first technique altering the passive waveguide cross section has been the approach followed herein, because photolithographic processes can be applied to all of the waveguide cross sections independent of its composition and substrate. Both chemical etching and ionic milling have been employed. Experience has shown that the iterative structure definition by ion milling produces a smoother undulated surface than by chemical etching, thus reducing scattering losses.

The photolithographic requirements to produce the contra-directional couplers are much more severe than employed to produce an electronic integrated circuit. The iterative period in the active waveguide walls

is 5 microns, whereas the period in the passive feedback waveguide is approximately 3 microns. Further, the grating must extend over dimensions of 10 cm preserving parallelism of the grating perturbation to a small fraction of the CO_2 wavelength. Further, the grating requirements must have optically smooth edges to prevent Rayleigh scattering. The average straightness or curvature requirements are identical to those of Fabry-Perot resonators of comparable dimensions. Conventional photolithographic practice, that is, production of the art work, its reduction and transfer to the final device, is capable of producing the required smooth lines. However, it has been considered impractical to follow this procedure and meet the requirements for parallelism of grating over the 10 cm length. Therefore, an interferometric (holographic), procedure has been pursued.[43-44]

Several techniques to produce gratings across a 10cm aperture have been investigated using both argon and krypton lasers in the visible region and photographic emulsions. A cadmium and krypton laser using the ultraviolet emission lines together with photoresist have also been investigated. The interferometer employed a beam expansion telescope and Twyman-Green interferometer configuration to produce gratings of 5.0 and 3.2 micron periods. The beam splitters are 10cm SiO_2 cubes split on the hypotenuse. Using the cadmium laser, insufficient power was available to expose the photoresist in a period less than one hour. The krypton laser provided sufficient power to expose the photoresist; however, the fluorescence due to the telescope aperture and the two beam splitters was sufficient to obscure the visibility of the fringes. The total path length including the various glasses was 22cm. Therefore, the further work in the ultraviolet and projection of fringes in the photoresist was discontinued. A krypton laser using the 5682Å emission line has been employed to produce the gratings in high resolution photographic plates followed by transfer to photoresist. Typical results of this operation are illustrated in the collage in Figure 21. Section A indicates the average density and shows evidence of Moire' pattern. The grating lines in Section A are vertical whereas the dominent Moire' pattern is horizontal. (The individual grating lines are probably not visible after the halftone printing.) An enlargement of the photographic emulsion is shown in Section B of

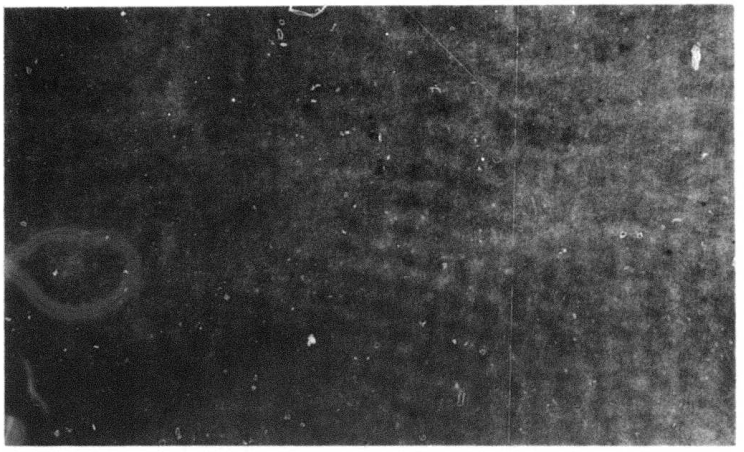

(a)

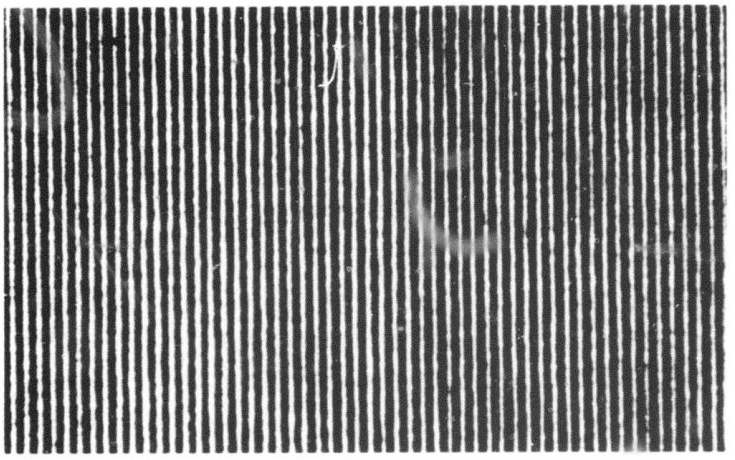

(b)

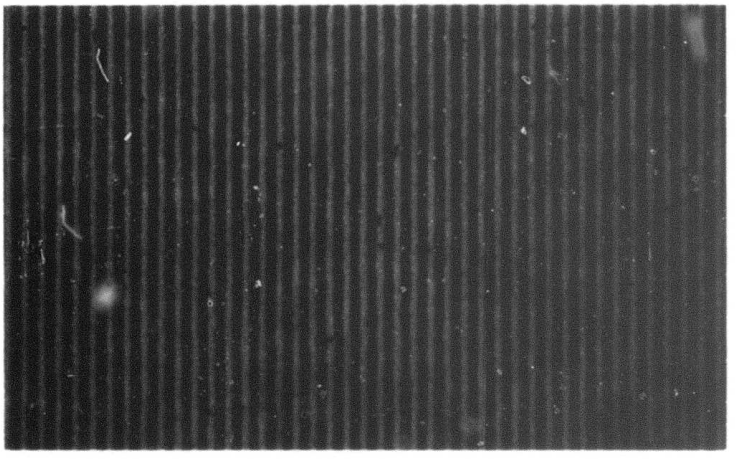

(c)

Figure 21. Photographic Collage of Gratings (See Text)

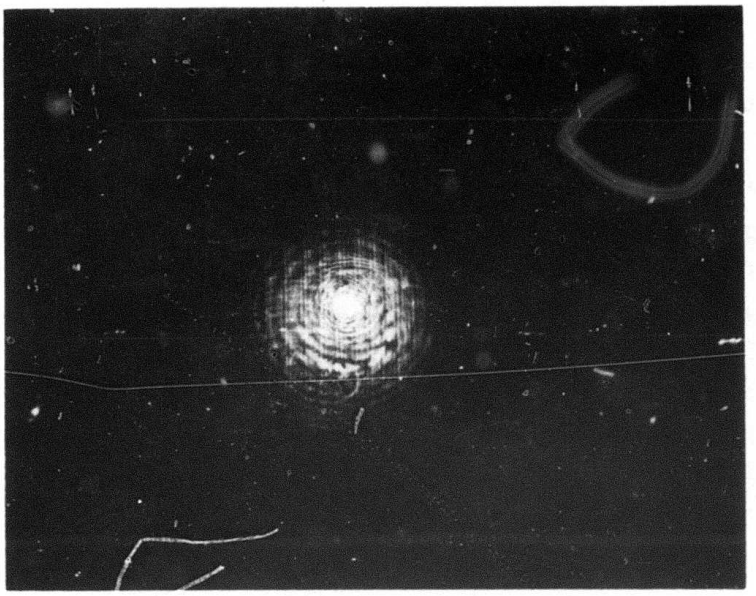

Figure 22. First Order Diffraction Holographic Reconstruction From Grating Shown in Figure 19

Figure 21. The transfer of this emulsion is photoresist on gold on chromium on a glass substrate is illustrated in Figure 21, Section C. The grating has been intentionally overexposed to reduce the white line width and providing sufficient density for the subsequent transfer to the photoresist. Inspection of Figure 21, Section B, indicates a gradual change of white line width (fringe null). Further, a fine structure modulation of the black lines is also apparent which transfers to the metallic grating in Section C.

As a means to qualitatively assess the grating efficiency, the grating shown in Figure 21 has been employed as a hologram to reconstruct the source in the first order as shown in Figure 22. The reconstructed image of Figure 22 shows a systematic pattern of wide angle sources which arise from defects in the cubic beam splitters. Further, the vertical fringes arise from interference in the polarization attenuator employed to balance the two beams. The other characteristic diffraction patterns can be traced to defects in the interferometer. The presence of the systematic sidelobes, the fringes

and wide angle scatter represent defects in the grating which contribute to the degradation of the efficiency.

The metallic grating illustrated in Figure 21C has been employed as one wall of a hollow planar waveguide. The other wall employed a glass sheet. The thickness of the waveguide was set at 100 microns. The transmission characteristics of a CO_2 laser beam through this waveguide with a grating on one surface is illustrated in Figure 23. The four dominant emission bands of the CO_2 laser are evident. The laser parameters are such that scanning from one rotational-vibrational line to the next does not entirely suppress its operation. Further, the experimental configuration and the scanning process excites modes in the waveguide as TE_3, TE_2, TE_1, TE_0 and TE_1, TE_2, TE_3. The effect of the grating is indicated at approximately 10.2 microns as a reduction in the transmission of the waveguide. A thermal detector was employed and its time constant is evident in the figure. The effect of the individual mode orders is not evident in this recording. Total reflection backward wave grating in this experiment is not possible because the hollow waveguide will simultaneously support many mode orders while only a single order is reflected by the grating. Because the scanning CO_2 emits discrete lines and because the grating reflectivity applies for a specific wavelength, phase matching to produce the backward reflection occurs at a selected unidentified mode order. Changes of the mode order represent changes of the angle of incidence.

A dominant portion of the effort has concentrated upon use of the metallic grating. This experience (absorption) strongly suggests that the grating should be an undulated surface changing the waveguide cross section. The depth of the undulated surface to produce the desired coupling coefficient is a factor requiring further investigation. The depth of modulation is determined by the preferential characteristics of the chemical etch or ion milling process. Thus far the modulation depths have been less than one micron whereas it is believed that they should be several times larger.

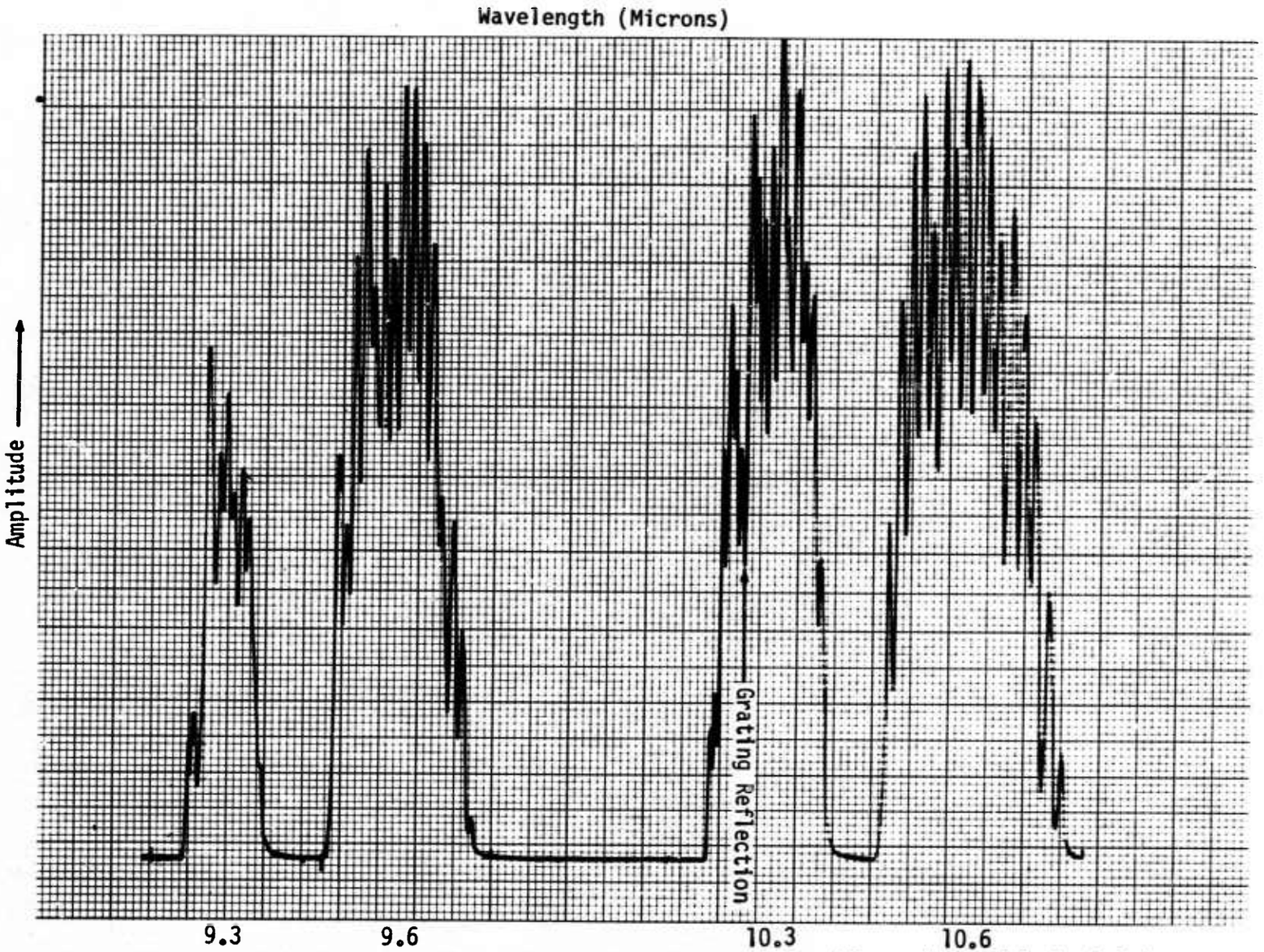

Figure 23. Recorded CO_2 Output Transmitted Through 100 Micron Linear Waveguide Containing a Grating Wall Reflecting at 10.2 Microns

III. REVIEW

A. CONCLUSIONS AND RECOMMENDATIONS

The effort thus far to develop and demonstrate a CO_2 gas laser employing an integrated optics approach continues to suggest its feasibility,[45] merits, and potential for including means for wide range electronic tuning. The first objective demonstrating this operation has thus far not been achieved, because the initial design parameters selected within which it is necessary to create a continuous uniform plasma discharge at relatively high pressure, has resulted in the production of a multiplicity of concentrated arcs. Thus, the necessary excited CO_2 plasma within the planar hollow active waveguide coupled with the feedback waveguide, has not been available for demonstration of laser operation.

All the techniques and concepts with the potential to produce a uniform plasma discharge in a thin waveguide at relatively high pressure have not been explored. Various means to produce a continuous uniform plasma discharge in the thin waveguide cross section is continuing to receive attention. At this juncture, it may be wise to perform a design tradeoff, relaxing the active waveguide thickness to obtain the necessary discharge while simultaneously accepting the aggravation of a more severe constraint upon the backward wave Bragg diffraction coupler efficiency and possible compromise of the wide tuning range capability. Because the plasma discharge chamber with its constriction by the thin active waveguide is not amenable to analysis, but instead requires an experimental investigation, estimates of the laser characteristics based upon the preceding analysis is not practical until the active waveguide configuration can be defined.

Pursuit of a design to produce a uniform plasma discharge in a thin planar waveguide is merited because:

1. the structure provides for continuous high velocity transverse flow of the gas mixture.
2. the planar waveguide configuration allows a high thermal conductive wall (BeO) to be in intimate contact with the plasma.
3. transverse flow and transverse excitation provides for a homogeneous pressure and temperature profile and thus a uniform laser collision-broadened emission line.

Preceding page blank

4. transverse excitation reducing the gap minimizes the requirement for high electric fields.

These features are not conveniently available in a waveguide capillary structure using a longitudinal flow excitation and coincident with the optical axis.

The characteristics of distributed-feedback lasers have been studied with regard toward their application to CO_2 planar-cavity-waveguide lasers. A coupled mode approach has been used to derive the coupling constants between contra-directional waves propagating in both the active gas waveguide and the passive feedback waveguide. It shows that the desired coupling may be readily achieved with small perturbations in either the refractive index of the dielectric feedback waveguide or by changes of its cross section. In addition, the complex reflection coefficients for distributed periodic structures have been computed which provide added insight into the behavior of DFB lasers. Production of the contra-directional couplers by interferometric techniques is satisfactory, however, requires ultraviolet fringe generation directly in the photoresist with an absolute minimum of optical elements.

A "longitudinal resonance" analysis using the coupled modes was used to derive complex eigenvalue equations giving threshold values of the laser oscillation frequency for distributed hetero-feedback DHFB lasers. It was shown that a DHFB structure having a central gap in a continuous feedback grating gives added control over the lasing spectrum by virtue of the fact that the frequency spacing of the primary lasing modes away from the Bragg frequency is strongly dependent upon the length of the central gap. For very small gap lengths and low gain, the longitudinal mode spacing can be several times larger than the spacing in a conventional Fabry-Perot of the same length. Thus, the nonuniform distributed feedback and the frequency selectivity of the contra-directional couplers provides an independent means to control the longitudinal mode period which can be employed to advantage in a high pressure CO_2 laser to affect a wider unambiguous tuning range.

The use of an integrated optics approach to construction is merited because of the attendant economies from batch and planar processing techniques.

Further, the planar construction with all circuit elements embedded in the substrate and superstrate surfaces provides an inherent stability. Further, the planar configuration coupled with traveling surface elastic waves provides a convenient alternative means for tuning the laser with a minimum of control power, because of the interaction throughout the entire active/passive waveguide region.

B. REFERENCES

1. J. D. Cobine, "Gaseous Conductors," Dover, New York, 1958

2. E. A. Marcatile and R. A. Schmeltzer, "Hollow Metallic and Dielectric Waveguides for Long Distance Optical Transmission and Lasers," BSTJ 43, 1783 (1964).

3. P. W. Smith, "A Waveguide Gas Laser," Appl. Phys. Letters 19, 132 (1971).

4. P. K. Cheo and H. G. Cooper, "Gain Characteristics of CO_2 Laser Amplifiers at 10.6 Microns," IEEE JQE 3, 79 (1967).

5. D. J. Franzen and R. J. Collins, "High Gain Small-Bore Cooled CO_2 Amplifier," IEEE JQE 6, 163, (1970).

6. E. G. Burkhardt, T. J. Bridges and P. W. Smith, BeO Capillary CO_2 Waveguide Laser," Optic Comm 6, 193 (1972).

7. T. J. Bridges, E. G. Burkhardt and P. W. Smith, "CO_2 Waveguide Lasers," Appl. Phys. Lett. 20, 403 (1972).

8. R. E. Jensen and M. S. Tobin, "CO_2 Waveguide Gas Laser," Appl. Phys. Lett. 20, 508 (1972).

9. J. J. Degnan, H. E. Walker, J. H. McElroy, N. McAvoy and T. Zagwodski, "A Curve-Fitting Technique for the Determination of Gain and Saturation Intensity in Homogeneously-Broadened Gas Lasers: Application to a Waveguide CO_2 Laser," Goddard Space Flight Center Report X-524-72-38) Oct 72.

10. H. Kogelnik and C. V. Shank, "Stimulated Emission in a Periodic Structure," Appl. Phys. Letters 18, 152 (1971).

11. C. V. Shank, J. E. Bjorkholm and H. Kogelnik, "Tunable Distributed-Feedback Dye Laser," Appl. Phys. Letters 18, 395 (1971).

12. J. E. Bjorkholm and C. V. Shank, "Distributed-Feedback Lasers in Thin-Film Optical Waveguide," OSA Topical Meeting on Integrated Optics - Guided Waves, Materials and Devices, Las Vegas, Nev., Feb. 7-10, 1972.

13. D. Marcuse, "Hollow Dielectric Waveguide for Distributed Feedback Lasers," IEEE, JQE 8, 661 (1972).

14. J. E. Bjorkholm and C. V. Shank, "Higher-Order Distributed Feedback Oscillators," Appl. Phys. Lett., 20, 306 (1972).

15. D. P. Schinke, R. G. Smith, E. G. Spencer and M. F. Galvin, "Thin Film Distributed Feedback Laser Fabricated by Ion Milling," Appl. Phys. Lett., 21, 494 (1972).

16. J. E. Bjorkholm and C. V. Shank, "Distributed-Feedback Lasers in Thin-Film Optical Waveguides," IEEE, JQE 8, 833 (1972).

17. P. Zory, "Laser Oscillation in Leaky Corrugated Optical Waveguides," Appl. Phys. Lett. 22, 125 (1973).

18. J. E. Bjorkholm, T. P. Sosnowski and C. V. Shank, "Distributed-Feedback Lasers in Optical Waveguides Deposited on Anisotropic Substrates," Appl. Phys. Lett. 22, 133 (1973).

19. H. Kogelnik and C. V. Shank, "Coupled-Wave Theory of Distributed Feedback Lasers," J. Appl. Phys. 43, 2317 (1972).

20. R. Shubert, "Collinear Interaction of Optical and Acoustics Guided Waves," Queen Mary College, Interim Report SRC Grant 9801, June 1972.

21. L. Kuhn, M. L. Dakss, P. F. Hiedrich and B. A. Scott, "Deflection of Optical Guided Wave by a Surface Acoustic Wave," Appl. Phys. Letters 17, 265 (1970).

22. L. Kuhn, P. F. Heidrich and E. G. Lean, "Optical Guided Wave Mode Conversion by an Acoustic Surface Wave," Appl. Phys. Letters 19, 428 (1970).

23. W. S. C. Chang, "Acousto-Optical Deflections in Thin Films," JQE 7, 167 (1971).

24. H. Kogelnik, C. V. Shank and J. E. Bjorkholm, "Hybrid Scattering in Periodic Waveguides," Appl. Phys. Lett. 22, 135, (1973).

25. P. W. Smith, "Mode Selection in Lasers," Proc. IEEE 60, 422 (1972).

26. F. W. Dabby, M. A. Saifi and A. Kestenbaum, "High-Frequency Cut-off Periodic Dielectric Waveguides," Appl. Phys. Lett. 22, 190 (1973).

27. S. Somelb and A. Yariv, "Phase-Matchable Nonlinear Optical Interactions in Periodic Thin Films," Appl. Phys. Lett., 21, 140 (1972).

28. F. W. Dabby, A. Kestenbaum and U. C. Paek, "Periodic Dielectric Waveguides," Optic Comm. 6, 125 (1972).

29. D. Marcuse, "Mode Conversion Caused by Surface Imperfections of a Dielectric Slab Waveguide, BSTJ 48, 3187 (1969).

30. C. F. Quate, C. D. W. Wilkinson, D. K. Winslow, "Interaction of Light and Microwave Sound," Proc. IEEE 53, 1604 (1965).

31. P. Zory, "Leaky Wave Thin-Film Laser," OSA Topical Meeting on Integrated Optics - Guided Waves, Materials and Devices, Las Vegas, Nev., Feb 7-10, 1972.

32. R. L. Abrams, "Hollow Dielectric Waveguide for Distributed Feedback Lasers," IEEE, JQE 8, 838 (1972).

33. A. N. Chester and R. L. Abrams, "Modes Losses in Hollow-Waveguide Lasers," Appl. Phys. Lett., 21, 576 (1972).

34. J. A. Beaulieu, "High Peak Power Gas Lasers," Proc. IEEE 59, 667 (1971).

35. W.E.K. Gibbs and R. McLeary, "Uniform Discharges in Flowing CO_2 Laser Mixtures at Atmospheric Pressure," Phys. Lett., 37A, 229 (1971).

36. D. L. Lyon, "Comparison of Theory and Equipment for Transversely Excited High Pressure CO_2 Lasers," IEEE, JQE 9, 139 (1973).

37. H. M. Lamberton and P. R. Pearson, "Improved Excitation Techniques for Atmospheric Pressure CO_2 Lasers," Electronics Lett., 7, 141 (1971).

38. A. C. Bckbreth and J. W. Davis, "The Cross Beam Electric-Discharge Convection Laser," IEEE, JQE 8, 139 (1972).

39. A. E. Hill, "Uniform Electrical Excitation of Large-Volume High Pressure Near-Sonic CO_2-N_2-H_e Flowstream," Appl. Phys. Lett. 18, 194 (1971).

40. R. J. Freiberg and P. O. Clark, "CO_2 Transverse-Discharge Lasers," IEEE, JQE 6, 105 (1970).

41. A. E. Hill, "Role of Thermal Effects and Fast Flow Power Scaling Techniques in CO_2-N_2-H_e Lasers," Appl. Phys. Lett. 16, 423 (1970).

42. R. McLeary and W.E.K. Gibbs, "Continuous-Wave CO_2 Laser at Atmospheric Pressure," VII International Quantum Electronics Conference Digest, 18 (1972).

43. H. Kogelnik and T. P. Sosnowski, "Holographic Thin Film Couplers," BSTJ 49, 1602 (1970).

44. H. Kogelnik, "Coupled Wave Theory for Thick Hologram Gartings," BSTJ 48, 2909 (1970).

45. S. Wang, "Proposal of Periodic Layered Waveguide Structures for Distributed Lasers," J. Appl. Phys. 44, 767 (1973).